

---

# Symbolic Music Generation with Fine-grained Interactive Textural Guidance

---

Tingyu Zhu\*

Haoyu Liu\*

Zhimin Jiang

Zeyu Zheng

## Abstract

The problem of symbolic music generation presents unique challenges due to the combination of limited data availability and the need for high precision in note pitch. To overcome these difficulties, we introduce Fine-grained Textural Guidance (FTG) within diffusion models to correct errors in the learned distributions. By incorporating FTG, the diffusion models improve the accuracy of music generation, which makes them well-suited for advanced tasks such as progressive music generation, improvisation and interactive music creation. We derive theoretical characterizations for both the challenges in symbolic music generation and the effect of the FTG approach. We provide numerical experiments and a demo page<sup>1</sup> for interactive music generation with user input to showcase the effectiveness of our approach.

## 1 Introduction

Symbolic music generation is a subfield of music generation that focuses on creating music in symbolic form, typically represented as sequences of discrete events such as notes, pitches, rhythms, and durations. These representations are analogous to traditional sheet music or MIDI files, where the structure of the music is defined by explicit musical symbols rather than audio waveforms. Symbolic music generation has a wide range of applications, including automatic composition, music accompaniment, improvisation, and arrangement. It can also play a significant role in interactive music systems, where a model can respond to user inputs or generate improvisational passages in real-time. A lot of progress has been made in the field of deep symbolic music generation in recent years; see Huang et al. (2018), Min et al. (2023), von Rütte et al. (2023), Wang et al. (2024) and Huang et al. (2024).

Despite recent progress, some unique challenges of symbolic music generation remain unresolved. A key obstacle is the scarcity of high-quality training data. While large audio datasets are readily available, symbolic music data is more limited, often due to copyright constraints. Additionally, unlike image generation, where the inaccuracy of a single pixel may not significantly affect overall quality, symbolic music generation demands high precision, especially in terms of pitch. In many tonal contexts, a single incorrect note can be glaringly obvious, even to less-trained ears.

As a partial motivation, we empirically observe the occurrence of “wrong notes” in existing state-of-the-art symbolic music generation models. We provide theoretical explanations for why these models may fail to avoid such errors. Apart from that, we find that many models encounter challenges in generating well-regularized accompaniment. While human-composed accompaniment often exhibits consistent patterns across bars and phrases, the generated symbolic accompaniment tends to vary significantly. These observations and theoretical discoveries highlight the need to ap-

---

\*Haoyu Liu and Tingyu Zhu contributed equally to this work. The authors gratefully acknowledge insightful discussions with Jinghai He, Ang Lv, Yifu Tang, Ziyu Wang, Gus Xia, Yaodong Yu and Yufeng Zheng. Correspondence to haoyuliu@berkeley.edu, tingyu\_zhu@berkeley.edu, jiangzhimin@aizeer.net and zy zheng@berkeley.edu.

<sup>1</sup>The demo page of this work is at <https://huggingface.co/spaces/haoyuliu00/InteractiveSymbolicMusic>

ply regularization through external guidance, rather than relying on the model to capture it entirely autonomously.

We then address the precision challenge in symbolic music generation building upon a diffusion model-based approach. Diffusion models can flexibly capture a wide variety of patterns in the data distribution, and therefore generate highly structured and detailed images (Ho et al., 2020). This flexibility makes diffusion models well-suited for piano roll-based symbolic music generation, where segmented piano rolls can be treated similarly to image data for processing. Further, guidance can be incorporated into the training process as background information and into the gradual denoising process to direct the sampling (Zhang et al., 2023b), enabling the design of specialized structures within diffusion models that integrate harmonic and rhythmic regularization. Our results in this work are summarized as follows:

- **Motivation:** We provide empirical observations and statistical theory evidence to reveal and characterize the precision and regularization challenges in symbolic music generation, underscoring the need for fine-grained guidance in training and generation.
- **Methodology:** We propose a controlled diffusion model for symbolic music generation that incorporates fine-grained harmonic and rhythmic guidance and regularization, in both the training and sampling processes. Even with limited training data, the model is capable of generating music with high accuracy and consistent rhythmic patterns.
- **Effectiveness:** We provide both theoretical and empirical evidence supporting the effectiveness of our approach, and further demonstrate the potential of the model to be applied in interactive music systems, where the model responds to user inputs and generates improvisational passages in real-time.

### 1.1 Related work

**Symbolic music generation.** Symbolic music generation literature can be classified based on the choice of data representation, among which the MIDI token-based representation adopts a sequential discrete data structure, and is often combined with sequential generative models such as Transformers and LSTMs. Examples of works using MIDI token-based data representation include Huang et al. (2018), Huang & Yang (2020), Ren et al. (2020), Choi et al. (2020), Hsiao et al. (2021), Lv et al. (2023) and von Rütte et al. (2023). While the MIDI token-based representation enables generative flexibility, it also introduces the challenge of simultaneously learning multiple dimensions that exhibit significant heterogeneity, such as the “pitch” dimension compared to the “duration” dimension. An alternative data representation used in music processing is the piano roll-based format. Many recent works adopt this data representation; see Min et al. (2023), Zhang et al. (2023a), Wang et al. (2024) and Huang et al. (2024) for example. Our work differs from their works in that we apply the textural guidance jointly in both the training and sampling process, and with an emphasis on enhancing real-time generation precision and speed. More detailed comparisons are provided in Appendix E, after we present a comprehensive description of our methodology.

**Controlled diffusion models.** Multiple works in controlled diffusion models are related to our work in terms of methodology. Specifically, we adopt the idea of classifier-free guidance in training and generation, see Ho & Salimans (2022). To control the sampling process, Chung et al. (2022), Song et al. (2023) and Novack et al. (2024) guide the intermediate sampling steps using the gradients of a loss function. In contrast, Dhariwal & Nichol (2021), Saharia et al. (2022), Lou & Ermon (2023) and Fishman et al. (2023) apply projection and reflection during the sampling process to straightforwardly incorporate data constraints. Different from these works, we design guidance for intermediate steps tailored to the unique characteristics of symbolic music data and generation. While the meaning of a specific pixel in an image is undefined until the entire image is generated, each position on a piano roll corresponds to a fixed time-pitch pair from the outset. This new context enables us to develop novel implementations and theoretical perspectives on the guidance approach.

## 2 Background: Diffusion models for piano roll generation

In this section, we introduce the data representation of piano roll. We then introduce the formulations of diffusion model, combined with an application on modeling the piano roll data.

Let  $\mathbf{M} \in \{0, 1\}^{L \times H}$  be a piano roll segment, where  $H$  is the pitch range and  $L$  is the number of time units in a frame. For example,  $H$  can be set as 128, representing a pitch range of 0 – 127, and  $L$  can be set as 64, representing a 4-bar segment with time signature 4/4 (4 beats per bar) and 16th-note resolution. Each element  $M_{lh}$  of  $\mathbf{M}$  ( $1 \leq l \leq L$ ,  $1 \leq h \leq H$ ) takes value 0 or 1, where  $M_{lh} = 1/0$  represents the presence/absence of a note at time index  $l$  and pitch  $h$ <sup>2</sup>. Since standard diffusion models are based on Gaussian noise, the output of the diffusion model is a continuous random matrix  $\mathbf{X} \in \mathbb{R}^{L \times H}$ , which is then projected to the discrete piano roll  $\mathbf{M}$  by  $M_{lh}(\mathbf{X}) = \mathbf{1}\{\mathbf{X}_{lh} \geq 1/2\}$ , where  $\mathbf{1}\{\cdot\}$  stands for the indicator function.

To model and generate the distribution of  $\mathbf{M}$ , denoted as  $P_{\mathbf{M}}$ , we use the the Denoising Diffusion Probabilistic Modeling (DDPM) formulation (Ho et al., 2020). This formulation uses two Markov processes: a forward process from  $t = 1$  to  $T$  corrupting data with increasing levels of Gaussian noise, and a backward process going from  $t = T$  to 1 removing noise from data. The objective of DDPM training, with specific choices of parameters and reparameterizations, is given as

$$\mathbb{E}_{t \sim \mathcal{U}[1, T], \mathbf{X}_0 \sim P_{\mathbf{M}}, \varepsilon \sim \mathcal{N}(0, \mathbf{I})} [\lambda(t) \|\varepsilon - \varepsilon_{\theta}(\mathbf{X}_t, t)\|^2], \quad (1)$$

where  $\mathbf{X}_t = \sqrt{\bar{\alpha}_t} \mathbf{X}_0 + \sqrt{1 - \bar{\alpha}_t} \varepsilon$  with hyperparameters  $\{\beta_t\}$ ,  $\bar{\alpha}_t = \prod_{s=0}^t (1 - \beta_s)$ , and  $\varepsilon_{\theta}$  is a deep neural network with parameter  $\theta$ . Moreover, according to the connection between diffusion models and score matching (Song & Ermon, 2019), the deep neural network  $\varepsilon_{\theta}$  can be used to derive an estimator of the score function  $\nabla_{\mathbf{X}_t} \log p_t(\mathbf{X}_t)$ . Specifically,  $\nabla_{\mathbf{X}_t} \log p_t(\mathbf{X}_t)$  can be approximated by  $-\varepsilon_{\theta}(\mathbf{X}_t, t) / \sqrt{1 - \bar{\alpha}_t}$ .

With the trained noise prediction network  $\varepsilon_{\theta}$ , the reverse sampling process can be formulated as (Song et al., 2020a):

$$\mathbf{X}_{t-1} = \sqrt{\bar{\alpha}_{t-1}} \left( \frac{\mathbf{X}_t - \sqrt{1 - \bar{\alpha}_t} \varepsilon_{\theta}(\mathbf{X}_t, t)}{\sqrt{\bar{\alpha}_t}} \right) + \sqrt{1 - \bar{\alpha}_{t-1} - \sigma_t^2} \varepsilon_{\theta}(\mathbf{X}_t, t) + \sigma_t \varepsilon_t, \quad (2)$$

where  $\sigma_t$  are hyperparameters chosen corresponding to equation 1, and  $\varepsilon_t$  is standard Gaussian noise at each step. When  $\sigma_t = \sqrt{\beta_{t-1}/\beta_t} \sqrt{1 - \bar{\alpha}_t/\bar{\alpha}_{t-1}}$ , the reverse process becomes the DDPM sampling process. Going backward in time from  $\mathbf{X}_T \sim \mathcal{N}(0, \mathbf{I})$ , the process yields the final output  $\mathbf{X}_0$ , which can be converted into a piano roll  $\mathbf{M}(\mathbf{X}_0)$ .

According to Song et al. (2020b), the DDPM forward process  $\mathbf{X}_t = \sqrt{\bar{\alpha}_t} \mathbf{X}_0 + \sqrt{1 - \bar{\alpha}_t} \varepsilon$  can be regarded as a discretization of the following SDE:

$$d\mathbf{X}_t = -\frac{1}{2} \beta(t) \mathbf{X}_t dt + \sqrt{\beta(t)} d\mathbf{W}_t, \quad (3)$$

and the corresponding denoising process takes the form of a solution to the following stochastic differential equation (SDE):

$$d\mathbf{X}_t = -\left[ \frac{1}{2} \beta(t) \mathbf{X}_t + \beta(t) \nabla_{\mathbf{X}_t} \log p_t(\mathbf{X}_t) \right] dt + \sqrt{\beta(t)} d\bar{\mathbf{W}}_t, \quad (4)$$

where  $\beta(t/T) = T\beta_t$  as  $T$  goes to infinity,  $\bar{\mathbf{W}}_t$  is the reverse time standard Wiener process, and  $\bar{\alpha}_t$  term should be replaced by its continuous version  $e^{-\int_0^t \beta(s) ds}$  (or  $e^{-\int_{t_0}^t \beta(s) ds}$  when early-stopping time  $t_0$  is adopted). The score function  $\nabla_{\mathbf{X}_t} \log p_t(\mathbf{X}_t)$  can be approximated by  $-\varepsilon_{\theta}(\mathbf{X}_t, t) / \sqrt{1 - e^{-\int_0^t \beta(s) ds}}$ .

**Remark 1.** Under the SDE formulation, the forward process terminates at a sufficiently large time  $T$ . Also, since the score functions blow up at  $t \approx 0$ , an early-stopping time  $t_0$  is commonly adopted to avoid such issue (Song & Ermon, 2020; Nichol & Dhariwal, 2021). When  $t_0$  is sufficiently small, the distribution of  $\mathbf{X}_{t_0}$  in the forward process is close enough to the real data distribution.

### 3 Challenges in symbolic music generation

While generative models have achieved significant success in text, image, and audio generation, the effective modeling and generation of symbolic music remains a relatively unexplored area. In this section, we introduce two major challenges of symbolic music generation.

<sup>2</sup>This is a slightly simplified representation model for the purpose of theoretical analysis, the specified version with implementation details is provided in Section 5.2

### 3.1 Harmonic precision

One challenge of symbolic music generation involves the high precision required for music generation. Unlike image generation, where a slightly misplaced pixel may not significantly affect the overall image quality, an “inaccurately” generated musical note can drastically affect the quality of a piece. This phenomenon can be more explicitly characterized and explained in the framework of harmonic analysis.

In music, harmony refers to the simultaneous sound of different notes that form a cohesive entity in the mind of the listener (Müller, 2015). The main constituent components of harmony are *chords*, which are musical constructs that typically consist of three or more notes. To create better harmonic alignment of the generated music, many literature of symbolic music generation, e.g., Min et al. (2023), von Rütte et al. (2023) and Wang et al. (2024), leverage chords as a pivoting element in data pre-processing, training and generation. In such works, chord-recognition algorithms are applied to training data to provide chords as conditions to the generative models. However, the complexity of harmonic analysis and chord recognition lies in the existence of nonharmonic tones. The nonharmonic tones are notes that are not part of the implied chord, but are often used in music as a combining element to create smooth melodic lines or transitions. The ambiguity of chords thus complicates automated chord recognition methods, often leading to errors.

Therefore, in addition to chord analysis, we also consider *key signatures*<sup>3</sup>, which establish the tonal center of music. Unlike nonharmonic tones, out-of-key notes are less common, at least in many genres<sup>4</sup>, and produce more noticeable dissonance. For instance, a  $G\sharp$  note is considered as out-of-key in a  $G\flat$  major context. While such notes might add an interesting tonal color when intentionally used by composers, they are usually perceived merely as mistakes when appearing in generative model outputs, see Figure 1 for example.



(a) Example from Mozart: Piano Sonata No. 5 in G major, K. 283, where  $C\sharp$  (out of the temporary D major key) and  $C\sharp$  appear simultaneously

(b) Example from the output of a diffusion model trained on POP909, the “wrong notes”  $A\sharp$  and  $G\sharp$  appear when  $G\flat$  should be the temporary key

Figure 1: Classical composers may use out-of-key notes to create interesting tonal color, but when such notes appear in the results of generative models, they almost always sound “strange”.

**Why generative models struggle with out-of-key notes** We now apply statistical theory to characterize why an out-of-key note is unlikely to be generated in a way that sounds “right” in context by a symbolic music generation model. We note that a summary of non-standard notations is provided in Appendix A. Denote the probability of  $M = M$  as  $P_M(M)$ , and the conditional probability of  $M = M$  under a specific key signature sequence  $\mathcal{K}$  as  $P_M(M|\mathcal{K})$ . Note that  $M$  is a specific realization of the piano roll segment, sampled from a data distribution.

Let  $\omega_{\mathcal{K}}(l) \subset \llbracket 1, H \rrbracket$  denote the subset of pitch values that are out of key  $\mathcal{K}(l)$ <sup>5</sup>, where  $\mathcal{K}(l)$  denotes the key signature at time  $l$ , and  $\mathbb{W}_{\mathcal{K}} = \{M \in \{0, 1\}^{L \times H} \mid \exists l \in \llbracket 1, L \rrbracket, \exists h \in \omega_{\mathcal{K}}(l), \text{ s.t. } M_{lh} = 1\}$  denotes the subset of piano rolls with the presence of notes-out-of-key for key sequence  $\mathcal{K}$ . The conditional probability that  $M$  has at least one note-out-of-key conditional on key  $K$  is  $P_M(w|\mathcal{K}) := \sum_{M \in \mathbb{W}_{\mathcal{K}}} P_M(M|\mathcal{K})$ .

<sup>3</sup>As a clarification, instead of assigning one single key to a piece or a big section, here we refer to each key associated with the *temporary tonic*.

<sup>4</sup>We note that out-of-key notes are more common in genres such as jazz and contemporary music. However, symbolic datasets rarely include music from these genres. Further, their inherent flexibility and the ambiguity in the assessment of quality present additional challenges for generative models. As a result, these genres are beyond the scope of this work.

<sup>5</sup>For example, if  $K$  stands for D major, since the a major scale is given as D, E, F#, G, A, B, C#, then the pitch values corresponding to E $\flat$ , F, G $\sharp$ , B $\flat$ , C are considered as notes out of the key. We additionally remark that due to the prevalence of the dominant seventh chord (D7), the note C may require special consideration.

As displayed in the examples of Figure 1, the inclusion of a note-out-of-key requires a meticulously crafted surrounding context in order to function as a legitimate accidental, rather than being perceived as a mere error. Let  $\mathbb{C}_\mathcal{K}^{h(l)}$  ( $l \in \llbracket 1, L \rrbracket$  and  $h(l) \subset \omega_\mathcal{K}(l)$ ) denote the subset of  $\mathbf{M}$  where there is a surrounding context accommodating the existence of out-of-key notes (referred to in brief as “*good context*”) for key  $\mathcal{K}$  at every point in  $h(l)$ . For simplicity, we consider the case of an out-of-key note in a fixed set of  $h(l)$ , and omit the subscripts  $l, h$ . Let  $P_\mathbf{M}(\mathbf{c}|\mathcal{K}) := \sum_{\mathbf{M} \in \mathbb{C}_\mathcal{K}} P_\mathbf{M}(\mathbf{M}|\mathcal{K})$ , denoting the probability of generating a “*good context*” for out-of-key notes, from the distribution of  $\mathbf{M}$  given key signature  $\mathcal{K}$ , and  $P_\mathbf{M}(\bar{\mathbf{c}}|\mathcal{K}) := \sum_{\mathbf{M} \in \{0,1\}^{L \times H} \setminus \mathbb{C}_\mathcal{K}} P_\mathbf{M}(\mathbf{M}|\mathcal{K}) = 1 - P_\mathbf{M}(\mathbf{c}|\mathcal{K})$ . Generative models estimate the underlying data distribution from the training data, and we denote the estimated distributions and probabilistic values with  $\hat{P}_\mathbf{M}(\cdot)$ . With these notations, we have

$$\hat{P}_\mathbf{M}(\bar{\mathbf{c}}|\mathbf{w}, \mathcal{K}) = \frac{\hat{P}_\mathbf{M}(\bar{\mathbf{c}}, \mathbf{w}|\mathcal{K})}{\hat{P}_\mathbf{M}(\mathbf{w}|\mathcal{K})} = \frac{\hat{P}_\mathbf{M}(\bar{\mathbf{c}}, \mathbf{w}|\mathcal{K})}{\hat{P}_\mathbf{M}(\mathbf{c}, \mathbf{w}|\mathcal{K}) + \hat{P}_\mathbf{M}(\bar{\mathbf{c}}, \mathbf{w}|\mathcal{K})}. \quad (5)$$

Note that  $\hat{P}_\mathbf{M}(\bar{\mathbf{c}}|\mathbf{w}, \mathcal{K})$  is the conditional probability of not having a “*good context*” to fit the wrong note, given that the wrong note  $\mathbf{w}$  is present in the generated output. When  $\hat{P}_\mathbf{M}(\bar{\mathbf{c}}, \mathbf{w}|\mathcal{K})$  is large compared with  $\hat{P}_\mathbf{M}(\mathbf{c}, \mathbf{w}|\mathcal{K})$ ,  $\hat{P}_\mathbf{M}(\bar{\mathbf{c}}|\mathbf{w}, \mathcal{K})$  can be close to 1.

To provide a rough idea, for a completely randomized generator, we have  $\hat{P}(\mathbf{c}, \mathbf{w}|\mathcal{K}) = |\mathbb{C}_\mathcal{K}| \cdot 2^{-(LH - |\sum_l \omega_\mathcal{K}(l)|)}$  and  $\hat{P}(\bar{\mathbf{c}}, \mathbf{w}|\mathcal{K}) = 1 - |\mathbb{C}_\mathcal{K}| \cdot 2^{-(LH - |\sum_l \omega_\mathcal{K}(l)|)}$ , where  $|\mathbb{C}_\mathcal{K}|$  is small because “*good context*” is rare in numbers,  $LH = 128 \times 128$ , and  $|\sum_l \omega_\mathcal{K}(l)| \approx \frac{5}{12} LH$ , making  $\hat{P}(\bar{\mathbf{c}}, \mathbf{w}|\mathcal{K})$  disproportionately larger than  $\hat{P}(\mathbf{c}, \mathbf{w}|\mathcal{K})$ . The following proposition 1 shows that  $\hat{P}_\mathbf{M}(\bar{\mathbf{c}}, \mathbf{w}|\mathcal{K})$  can still be large for trained models.

**Proposition 1.** *Consider approximating  $P_\mathbf{M}$  with the distribution of a continuous random variable  $\mathbf{X}$ . Given  $n$  i.i.d. data  $\{\mathbf{X}^i\}_{i=1}^n \sim p_\mathbf{X}$ , and  $\{\mathbf{M}^i\}_{i=1}^n$  be given by  $\mathbf{M}_{lh}^i = \mathbf{1}\{\mathbf{X}_{lh}^i \geq 1/2\}$ . Let  $\mathcal{P}_\delta$  be a distribution class restricted by  $P_\mathbf{M}(\bar{\mathbf{c}}, \mathbf{w}|\mathcal{K}) = \delta$ , with mild assumptions on the estimator  $\hat{p}_\mathbf{X}$  and  $\mathcal{P}_\delta$  (details in Appendix C.1), we have  $\exists C > 0$  such that  $\forall n$ ,*

$$\inf_{\hat{p}_\mathbf{X}} \sup_{p_\mathbf{X} \in \mathcal{P}_\delta} \mathbb{E}_{\{\mathbf{M}^i\}_{i=1}^n \sim P_\mathbf{M}} \hat{P}_\mathbf{M}(\bar{\mathbf{c}}, \mathbf{w}|\mathcal{K}) \geq C \cdot n^{-\frac{1}{LH+2}} - \delta, \quad (6)$$

where  $\hat{P}_\mathbf{M}$  is derived from  $\hat{p}_\mathbf{X}$  via the connection  $\hat{\mathbf{M}}_{lh}^i = \mathbf{1}\{\hat{\mathbf{X}}_{lh}^i \geq 1/2\}$ .

Note that  $P_\mathbf{M}(\bar{\mathbf{c}}, \mathbf{w}|\mathcal{K}) = \delta$  is very small, so equation 6 provides a characterization of the decay rate of  $\hat{P}_\mathbf{M}(\bar{\mathbf{c}}, \mathbf{w}|\mathcal{K})$  with  $n$ , when  $\hat{P}_\mathbf{M}(\bar{\mathbf{c}}, \mathbf{w}|\mathcal{K})$  is relatively large comparing with  $\delta$ , corresponding to the situation of our concern.

Proposition 1 outlines the statistical inefficiency for any continuous estimator for piano rolls (including e.g., GANs and VAEs applying Gaussian noise) in terms of modeling the out-of-key notes, although taking supremum of  $p_\mathbf{X} \in \mathcal{P}_\delta$  considers the worst-case scenario. The order of  $O(n^{-1/(LH+2)})$  shows how the scarcity of data is exacerbated by the curse of dimensionality, where  $LH$  is often set as  $128 \times 128$  in a piano roll segment. The proof of proposition 1 follows from Fu et al. (2024), and is given in Appendix C.1. We additionally remark that while discrete probabilistic estimators are not included in the analysis, empirical results suggest that Gaussian-based diffusion models outperform them in several aspects, particularly in the quality of generated music (Wang et al., 2024; Huang et al., 2024).

### 3.2 Rhythmic regularity

A second observation regarding symbolic music generation models is their tendency to produce irregular rhythmic patterns. While many composers typically maintain consistent rhythmic patterns across consecutive measures within a 4-bar phrase, particularly in the accompaniment, such variations frequently appear in the generated accompaniment of symbolic music generative models.

Such phenomena can be explained by the scarcity of data and the high dimensionality hindering the model’s ability to capture correlations between different bars, even within a single generated section. Additionally, the irregularity in generated patterns can stem from the presence of irregular samples in many existing MIDI datasets. Without a sufficient quantity of data exhibiting clear correlations and repetition across measures, it is unlikely that the model will self-generate more human-like and consistent accompaniment patterns.



Figure 2: Example of an accompaniment segment generated by a diffusion model depicting high variation in rhythmic pattern. Examples of human-composed accompaniment are provided in the appendix B for comparison.

## 4 Methodology: Fine-grained textural guidance

In the previous section 3, we identified the unique challenges in symbolic music generation arising from the distinctive characteristics and specific requirements of symbolic music data. Together with the scarcity of available high-quality data for training, this underscores the need for fine-grained external control and regularization in generating symbolic music. In this section, we present our methodology of applying fine-grained regularization guidance to improve the quality and stability of the generated symbolic music.

An important characteristic of piano-roll data, crucial for designing fine-grained control, is that each position corresponds to a fixed time-pitch pair, providing a clear interpretation even before the full sample is generated. This characteristic contrasts with other data types, such as image data, where the meanings of pixel values remain unclear until the image is fully generated, and individual pixels can only be interpreted together with surrounding pixels in a convoluted manner. Therefore, we accordingly design fine-grained conditioning and sampling correction/regularization, altogether referred to as *Fine-grained Textural Guidance* (FTG) that leverage this characteristic of the piano roll data. We use “texture” to refer to harmony and rhythm together.

### 4.1 Fine-grained conditioning in training

We train a conditional diffusion model with fine-grained harmonic ( $\mathcal{C}$ , required) and rhythmic ( $\mathcal{R}$ , optional) conditions, which are provided to the diffusion models in the form of a piano roll  $M^{\text{cond}}$ . We provide illustration of  $M^{\text{cond}}(\mathcal{C}, \mathcal{R})$  and  $M^{\text{cond}}(\mathcal{C})$  via examples in Figure 3. The mathematical descriptions are provided in Appendix D.

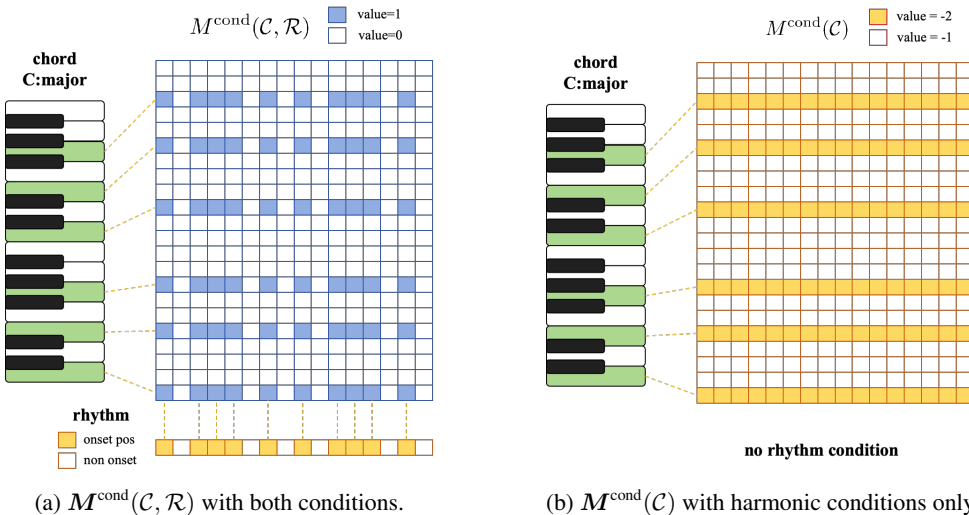


Figure 3: An illustrative example of  $M^{\text{cond}}(\mathcal{C}, \mathcal{R})$  and  $M^{\text{cond}}(\mathcal{C})$ .

While conditional generation enhances output stability, it comes at the cost of reduced sample variation, particularly when rhythmic conditions are applied. Therefore, to enable the model to generate under varying levels of conditioning, including unconditional generation, we implement the idea

of classifier-free guidance, and randomly apply conditions with or without rhythmic pattern in the process of training. Namely, the training loss is modified from equation 1 and given as

$$\mathbb{E}_{t, \varepsilon, \mathbf{X}_0} [\lambda_1(t) \|\varepsilon - \varepsilon_\theta(\mathbf{X}_t, \mathbf{M}^{\text{cond}}(\mathcal{C}), t)\|^2 + \lambda_2(t) \|\varepsilon - \varepsilon_\theta(\mathbf{X}_t, \mathbf{M}^{\text{cond}}(\mathcal{C}, \mathcal{R}), t)\|^2], \quad (7)$$

where  $\lambda_1(t)$  and  $\lambda_2(t)$  are hyper-parameters. Note that both  $\mathbf{M}^{\text{cond}}(\mathcal{C})$  and  $\mathbf{M}^{\text{cond}}(\mathcal{C}, \mathcal{R})$  are derived from  $\mathbf{X}_0$  via pre-designed chord recognition and rhythmic identification algorithms.

The guided noise prediction at timestep  $t$  is then computed as

$$\begin{aligned} \varepsilon_\theta(\mathbf{X}_t, t | \mathcal{C}, \mathcal{R}) = & \varepsilon_\theta(\mathbf{X}_t, \mathbf{M}^{\text{cond}}(\mathcal{C}), t) \\ & + w \cdot [\varepsilon_\theta(\mathbf{X}_t, \mathbf{M}^{\text{cond}}(\mathcal{C}, \mathcal{R}), t) - \varepsilon_\theta(\mathbf{X}_t, \mathbf{M}^{\text{cond}}(\mathcal{C}), t)], \end{aligned} \quad (8)$$

where  $w$  is the weight parameter. Note that the general formulation  $\varepsilon_\theta(\mathbf{X}_t, t | \mathcal{C}, \mathcal{R})$  includes the case where rhythmic guidance is not provided ( $\mathcal{R} = \emptyset$ ), and  $w$  in equation 8 is set as 0.

## 4.2 Fine-grained control in sampling process

As indicated by proposition 1 and empirical observations, providing chord conditions to model cannot prevent them from generating “wrong notes” that do not belong to the indicated key signature and context. Likewise, the rhythmic conditions also do not guarantee precise alignment with the provided rhythm. Therefore, in this section we design a fine-grained sampling control to enhance the precision of generation.

We aim to incorporate control at intermediate sampling steps to ensure the elimination of out-of-key notes, preventing noticeable inharmonious effects. Given key signature sequence  $\mathcal{K}$  derived from chord condition  $\mathcal{C}$ , let  $\omega_{\mathcal{K}}(\mathbf{l}) := \{l, \omega_{\mathcal{K}}(l)\}_{l=1}^L$  denote all out-of-key positions implied by  $\mathcal{K}$ , the generated piano-roll  $\widehat{\mathbf{M}}$  is expected to satisfy  $\widehat{\mathbf{M}} \in \{0, 1\}^{L \times H} \setminus \mathbb{W}_{\mathcal{K}}$ , i.e.,  $\widehat{M}_{lh} = 0$ , for all  $(l, h) \in \omega_{\mathcal{K}}(\mathbf{l})$ . In other words, the desired constrained distribution for generated  $\widehat{\mathbf{X}}_0$  satisfies

$$P \left( \widehat{\mathbf{X}}_0 \in \mathbb{W}'_{\mathcal{K}} := \{ \mathbf{X} \mid \exists (l, h) \in \omega_{\mathcal{K}}(\mathbf{l}), \text{ s.t. } X_{lh} > 1/2 \} \mid \mathcal{K} \right) = 0. \quad (9)$$

Note that in the backward sampling equation 2 that derives  $\mathbf{X}_{t-1}$  from  $\mathbf{X}_t$ , we have for the first term (Song et al., 2020a; Chung et al., 2022)

$$\left( \frac{\mathbf{X}_t - \sqrt{1 - \bar{\alpha}_t} \widehat{\varepsilon}_\theta(\mathbf{X}_t, t)}{\sqrt{\bar{\alpha}_t}} \right) = \text{“predicted } \mathbf{X}_0\text{”} = \widehat{\mathbb{E}}[\mathbf{X}_0 | \mathbf{X}_t], \quad t = T, T-1, \dots, 1. \quad (10)$$

It is suggested in proposition 1 that the major reason leading to generated wrong notes lies in the incorrect estimation of probability density  $\widehat{p}_X$ , which in turn affects the corresponding score function  $\nabla_{\mathbf{X}_t} \log \widehat{p}_t(\mathbf{X}_t)$ . The equivalence  $\nabla_{\mathbf{X}_t} \log \widehat{p}_t(\mathbf{X}_t) = -\widehat{\varepsilon}_\theta(\mathbf{X}_t, t)/\sqrt{1 - \bar{\alpha}_t}$  therefore inspires us to project  $\widehat{\mathbb{E}}[\mathbf{X}_0 | \mathbf{X}_t]$  to the  $\mathcal{K}$ -constrained domain  $\mathbb{R}^{L \times H} \setminus \mathbb{W}'_{\mathcal{K}}$  by adjusting the value of  $\widehat{\varepsilon}_\theta(\mathbf{X}_t, t)$  at every sampling step  $t$ . This adjustment is interpreted as a correction of the estimated score.

Specifically, using the notations in 4.1, at each sampling step  $t$ , we replace the guided noise prediction  $\widehat{\varepsilon}_\theta(\mathbf{X}_t, t | \mathcal{C}, \mathcal{R})$  with  $\tilde{\varepsilon}_\theta(\mathbf{X}_t, t | \mathcal{C}, \mathcal{R})$  such that

$$\begin{aligned} \tilde{\varepsilon}_\theta(\mathbf{X}_t, t | \mathcal{C}, \mathcal{R}) = & \arg \min_{\varepsilon} \|\varepsilon - \widehat{\varepsilon}_\theta(\mathbf{X}_t, t | \mathcal{C}, \mathcal{R})\| \\ \text{s.t.} \quad & \left( \frac{\mathbf{X}_t - \sqrt{1 - \bar{\alpha}_t} \varepsilon}{\sqrt{\bar{\alpha}_t}} \right) \in \mathbb{R}^{L \times H} \setminus \mathbb{W}'_{\mathcal{K}}. \end{aligned} \quad (11)$$

The element-wise formulation of  $\tilde{\varepsilon}_\theta(\mathbf{X}_t, t | \mathcal{C}, \mathcal{R})$  is given as follows, with calculation details provided in Appendix C.2.

$$\begin{aligned} \tilde{\varepsilon}_{\theta, lh}(\mathbf{X}_t, t | \mathcal{C}, \mathcal{R}) = & \mathbf{1}\{(l, h) \notin \omega_{\mathcal{K}}(\mathbf{l})\} \cdot \widehat{\varepsilon}_{\theta, lh}(\mathbf{X}_t, t | \mathcal{C}, \mathcal{R}) \\ & + \mathbf{1}\{(l, h) \in \omega_{\mathcal{K}}(\mathbf{l})\} \cdot \max \left\{ \widehat{\varepsilon}_{\theta, lh}(\mathbf{X}_t, t | \mathcal{C}, \mathcal{R}), \frac{1}{\sqrt{1 - \bar{\alpha}_t}} \left( X_{t, lh} - \frac{\sqrt{\bar{\alpha}_t}}{2} \right) \right\}. \end{aligned} \quad (12)$$

Plugging the corrected noise prediction  $\tilde{\varepsilon}_\theta(\mathbf{X}_t, t | \mathcal{C}, \mathcal{R})$  into equation 2, we derive the corrected  $\tilde{\mathbf{X}}_{t-1}$ . The sampling process is therefore summarized as the following Algorithm 1.

---

**Algorithm 1:** DDPM sampling with fine-grained harmonic control

---

**Input:** Input parameters: forward process variances  $\beta_t$ ,  $\bar{\alpha}_t = \prod_{s=1}^t \beta_s$ , backward noise scale  $\sigma_t$ , chord condition  $\mathcal{C}$ , rhythmic condition  $\mathcal{R}$  (can be null), key signature guidance  $\mathcal{K}$

**Output:** generated piano roll  $\tilde{\mathbf{M}} \in \{0, 1\}^{L \times H}$

- 1  $\mathbf{X}_T \sim \mathcal{N}(0, \mathbf{I})$ ;
- 2 **for**  $t = T, T-1, \dots, 1$  **do**
- 3   | Compute guided noise prediction  $\hat{\varepsilon}_\theta(\mathbf{X}_t, t | \mathcal{C}, \mathcal{R})$ ;
- 4   | Perform noise correction: derive  $\tilde{\varepsilon}_\theta(\mathbf{X}_t, t | \mathcal{C}, \mathcal{R})$  using equation 12;
- 5   | Compute  $\tilde{\mathbf{X}}_{t-1}$  by plugging the corrected noise  $\tilde{\varepsilon}_\theta(\mathbf{X}_t, t | \mathcal{C}, \mathcal{R})$  into equation 2
- 6 **end**
- 7 Convert  $\tilde{\mathbf{X}}_0$  into piano roll  $\tilde{\mathbf{M}}$
- 8 **return**  $output$ ;

---

Note that at the final step  $t = 0$ , the noise correction directly projects  $\tilde{\mathbf{X}}_0$  to  $\mathbb{R}^{L \times H} \setminus \mathbb{W}'_{\mathcal{K}}$ , ensuring the probabilistic constraint 9. A natural concern is that enforcing precise fine-grained control over generated samples may disrupt the learned local patterns. The following proposition 2, proved in C.3, provides an upper bound that quantifies this potential effect.

**Proposition 2.** *Under the SDE formulation in equation 3 and equation 4, given an early-stopping time  $t_0$ <sup>6</sup>, if*

$$\mathbb{E}_{\mathbf{X}_t \sim p_t} [\|\varepsilon^*(\mathbf{X}_t, t) - \varepsilon_\theta(\mathbf{X}_t, t)\|^2] \leq \delta \quad (13)$$

for all  $t$ , where  $\varepsilon^*(\mathbf{X}_t, t)$  is the optimal solution of the DDPM training objective (1), then we have

$$KL(\tilde{p}_{t_0} | p_{t_0}) \leq \frac{\delta}{2} \int_{t_0}^T \frac{\beta(t)}{\sqrt{1 - e^{- \int_{t_0}^t \beta(s) ds}}} dt, \quad KL(\tilde{p}_{t_0} | \hat{p}_{t_0}) \leq \frac{\delta}{2} \int_{t_0}^T \frac{\beta(t)}{\sqrt{1 - e^{- \int_{t_0}^t \beta(s) ds}}} dt,$$

where  $p_{t_0}$  is the distribution of  $\mathbf{X}_{t_0}$  in the forward process,  $\hat{p}_{t_0}$  is the distribution of  $\hat{\mathbf{X}}_{t_0}$  generated by the diffusion sampling process without noise correction, and  $\tilde{p}_{t_0}$  is the distribution of  $\tilde{\mathbf{X}}_{t_0}$  generated by the fine-grained noise correction.

Proposition 2 provides upper bounds for the distance between the controlled distribution and the uncontrolled distribution, as well as between the controlled distribution and the ground truth.

## 5 Experiments

In this section, we present experiments, including empirical observations of generated examples and numerical comparisons with baseline models, to demonstrate the effectiveness of our fine-grained guidance approach. We additionally create a demopage<sup>7</sup> for demonstration, which allows for fast and stable interactive music creation with user-specified input guidance.

### 5.1 Empirical Observations

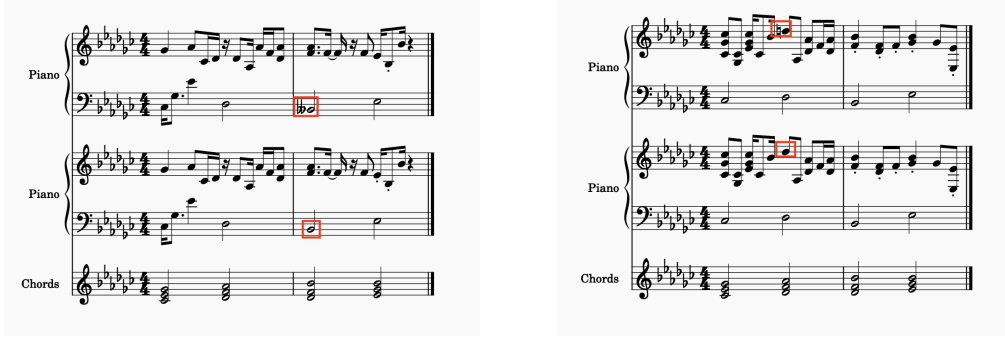
In this section, we provide empirical examples of how model output is reshaped by fine-grained correction in Figure 4. Notably, harmonic control not only helps the model eliminate incorrect notes, but also guides it to replace them with correct ones.

### 5.2 Numerical Experiments

We focus our numerical experiments on accompaniment generation given melody and chord conditions. We briefly introduce the data representation and our model architecture in Section 5.2.1. We compare with two state-of-art baselines: 1) WholeSongGen (Wang et al., 2024) and 2) GETMusic (Lv et al., 2023).

<sup>6</sup>As stated in Remark 1, we adopt the early-stopping time to avoid the blow-up of score function. When  $t_0$  is sufficiently small, the distributions at  $t = t_0$  are close enough to the distributions at  $t = 0$ .

<sup>7</sup>See <https://huggingface.co/spaces/haoyuliu00/InteractiveSymbolicMusic>. We note that slow performance may result from Huggingface resource limitations and network latency. Locally, it only takes 0.4 seconds on a NVIDIA RTX A6000 Ada Generation GPU and 4 seconds on a local CPU to generate a 4-measure phrase with user-specified guidance.



(a) An example of replacing a wrong note  $B_{bb}$  with the in-key note  $B_b$

(b) An example of replacing a wrong note  $D\#$  with the in-key note  $D_b$

Figure 4: Examples resulting from symbolic music generation with FTG. The first track is generated without key-signature control in sampling, the second track is generated with key-signature sampling control. The third track presents the chord condition. In each subfigure, the tracks are generated with the same conditions and the same set of noise.

### 5.2.1 Data Representation and Model Architecture

We represent music scores as image-like piano rolls for the generation target  $\mathbf{X}$ , which is represented by a matrix of shape  $2 \times L \times 128$  under the resolution of a 16th note, where  $L$  represents the total length of the music piece, and the two channels represent note onset and sustain, respectively. In our experiments, the model takes inputs with  $L = 64$ , corresponding to a 4-measure piece under time signature 4/4. Longer music pieces can be generated autoregressively using the inpainting method. The backbone of our model is a 2D UNet with spatial attention.

The condition matrix  $\mathbf{M}^{\text{cond}}$  is also represented by a piano roll matrix of shape  $2 \times L \times 128$ , with the same resolution and length as that of the generation target  $\mathbf{X}$ . As stated in Section 4.1, our model can take two kinds of condition matrix: one with both harmonic and rhythm conditions ( $\mathbf{M}^{\text{cond}}(\mathcal{C}, \mathcal{R})$ ), the other with harmonic condition only ( $\mathbf{M}^{\text{cond}}(\mathcal{C})$ ). For the accompaniment generation experiments, we provide melody as an additional condition. Detailed construction of the condition matrices are provided in Appendix F.

### 5.2.2 Dataset

We use the POP909 dataset (Wang et al., 2020a) for training and evaluation. This dataset consists of 909 MIDI pieces of pop songs, each containing lead melodies, chord progression, and piano accompaniment tracks. We exclude 29 pieces that are in triple meter, leaving 880 pieces for our experiments. 90% of the data are used to train our model, and the remaining 10% are used for evaluation. In the training process, we split all the midi pieces into 4-measure non-overlapping segments (corresponding to  $L = 64$  under the resolution of a 16th note), which in total generates 15761 segments in the entire training set.

### 5.2.3 Training and Sampling Details

We set diffusion timesteps  $T = 1000$  with  $\beta_0 = 8.5e-4$  and  $\beta_T = 1.2e-2$ . We use AdamW optimizer with a learning rate of  $5e-5$ ,  $\beta_1 = 0.9$ , and  $\beta_2 = 0.999$ . We train for 10 epochs with batch size 16, resulting in 985 steps in each epoch.

To speed up the sampling process, we select a sub-sequence of length 10 from  $\{1, \dots, T\}$  and apply the accelerated sampling process in Song et al. (2020a). It takes 0.4 seconds to generate the 4-measure accompaniment on a NVIDIA RTX 6000 Ada Generation GPU.

### 5.2.4 Task and Baseline Models

We consider accompaniment generation task based on melody and chord progression. We compare the performance of our model with two baseline models: 1) WholeSongGen (Wang et al., 2024) and

2) GETMusic (Lv et al., 2023). WholeSongGen is a hierarchical music generation framework that leverages cascaded diffusion models to generate full-length pop songs. It introduces a four-level computational music language, with the last level being accompaniment. The model for the last level can be directly used to generate accompaniment given music phrases, lead melody, and chord progression information. GETMusic is a versatile music generation framework that leverages a discrete diffusion model to generate tracks based on flexible source-target combinations. The model can also be directly applied to generate piano accompaniment conditioning on melody and chord. Since these baseline models do not support rhythm control, to ensure comparability, we will use the  $\mathcal{M}^{\text{cond}}(\mathcal{C})$  without rhythm condition in our model.

### 5.2.5 Evaluation

We generate accompaniments for the 88 MIDI pieces in our evaluation dataset.<sup>8</sup> We introduce the following objective metrics to evaluate the generation quality of different methods:

(1) *Chord Progression Similarity* We use a rule-based chord recognition method from Dai et al. (2020) to recognize the chord progressions of the generated accompaniments and the ground truth accompaniments. Then we split all chord progressions into non-overlapping 2-measure segments, and encode each segment into a 256-d latent space use a pre-trained disentangled VAE (Wang et al., 2020b). We then calculate the pairwise cosine similarities of the generated segments and the ground truth segments in the latent space. The average similarities with their 95% confidence intervals are shown in the first column of Table 1. The results indicate that our method significantly outperforms the other two baselines in chord accuracy.

(2) *Feature Distribution Overlapping Area* We assess the Overlapping Area (OA) of the distributions of some musical features in the generated and ground truth segments, including note pitch, duration, and note density<sup>9</sup>. Similarly, we split both the generated accompaniments and the ground truth into non-overlapping 2-measure segments. Following von Rütte et al. (2023), for each feature  $f$ , we calculate the macro overlapping area (MOA) in segment-level feature distributions so that the metric also considers the temporal order of the features. MOA is defined as

$$MOA(f) = \frac{1}{N} \sum_{i=1}^N \text{overlap}(\pi_i^{\text{gen}}(f), \pi_i^{\text{gt}}(f)),$$

where  $\pi_i^{\text{gen}}(f)$  is the distribution of feature  $f$  in the  $i$ -th generated segment, and  $\pi_i^{\text{gt}}(f)$  is the distribution of feature  $f$  in the  $i$ -th ground truth segment. The MOA's for different methods are shown in the last 3 columns in Table 1. Our method significantly outperforms the baselines in terms of pitch distribution. The performance on duration and note density distribution is slightly lower than WholeSongGen, which makes sense because the WholeSongGen model leverages more background information<sup>10</sup>.

Methods	Chord Similarity	OA(pitch)	OA(duration)	OA(note density)
FTG	<b>0.715 ± 0.007</b>	<b>0.579 ± 0.005</b>	0.548 ± 0.006	0.714 ± 0.005
WholeSongGen	0.611 ± 0.010	0.471 ± 0.006	<b>0.586 ± 0.005</b>	<b>0.726 ± 0.005</b>
GETMusic	0.394 ± 0.012	0.323 ± 0.010	0.377 ± 0.011	0.661 ± 0.011

Table 1: Evaluation of the Similarity with Ground Truth for all methods

## References

Sitan Chen, Sinho Chewi, Jerry Li, Yuanzhi Li, Adil Salim, and Anru R Zhang. Sampling is as easy as learning the score: theory for diffusion models with minimal data assumptions. *arXiv preprint arXiv:2209.11215*, 2022.

<sup>8</sup>The WholeSongGen model from Wang et al. (2024) is also trained on the POP909 dataset. Our evaluation set is a subset of their test set so there is no in-sample evaluation issue on their model.

<sup>9</sup>Note density is the number of onset notes at each time

<sup>10</sup>Apart from melody and chord, the accompaniment generation model in WholeSongGen also takes music phrases and reduced melody as conditions.

Kristy Choi, Curtis Hawthorne, Ian Simon, Monica Dinculescu, and Jesse Engel. Encoding musical style with transformer autoencoders. In *International conference on machine learning*, pp. 1899–1908. PMLR, 2020.

Hyungjin Chung, Jeongsol Kim, Michael T Mccann, Marc L Klasky, and Jong Chul Ye. Diffusion posterior sampling for general noisy inverse problems. *arXiv preprint arXiv:2209.14687*, 2022.

Shuqi Dai, Huan Zhang, and Roger B Dannenberg. Automatic analysis and influence of hierarchical structure on melody, rhythm and harmony in popular music. *arXiv preprint arXiv:2010.07518*, 2020.

Prafulla Dhariwal and Alexander Nichol. Diffusion models beat gans on image synthesis. *Advances in neural information processing systems*, 34:8780–8794, 2021.

Nic Fishman, Leo Klarner, Valentin De Bortoli, Emile Mathieu, and Michael Hutchinson. Diffusion models for constrained domains. *arXiv preprint arXiv:2304.05364*, 2023.

Hengyu Fu, Zhuoran Yang, Mengdi Wang, and Minshuo Chen. Unveil conditional diffusion models with classifier-free guidance: A sharp statistical theory. *arXiv preprint arXiv:2403.11968*, 2024.

Jonathan Ho and Tim Salimans. Classifier-free diffusion guidance. *arXiv preprint arXiv:2207.12598*, 2022.

Jonathan Ho, Ajay Jain, and Pieter Abbeel. Denoising diffusion probabilistic models. *Advances in neural information processing systems*, 33:6840–6851, 2020.

Wen-Yi Hsiao, Jen-Yu Liu, Yin-Cheng Yeh, and Yi-Hsuan Yang. Compound word transformer: Learning to compose full-song music over dynamic directed hypergraphs. In *Proceedings of the AAAI Conference on Artificial Intelligence*, volume 35, pp. 178–186, 2021.

Cheng-Zhi Anna Huang, Ashish Vaswani, Jakob Uszkoreit, Noam Shazeer, Ian Simon, Curtis Hawthorne, Andrew M Dai, Matthew D Hoffman, Monica Dinculescu, and Douglas Eck. Music transformer. *arXiv preprint arXiv:1809.04281*, 2018.

Yu-Siang Huang and Yi-Hsuan Yang. Pop music transformer: Beat-based modeling and generation of expressive pop piano compositions. In *Proceedings of the 28th ACM international conference on multimedia*, pp. 1180–1188, 2020.

Yujia Huang, Adishree Ghatare, Yuanzhe Liu, Ziniu Hu, Qinsheng Zhang, Chandramouli S Sastry, Siddharth Gururani, Sageev Oore, and Yisong Yue. Symbolic music generation with non-differentiable rule guided diffusion. *arXiv preprint arXiv:2402.14285*, 2024.

Ioannis Karatzas and Steven Shreve. *Brownian motion and stochastic calculus*, volume 113. Springer Science & Business Media, 1991.

Aaron Lou and Stefano Ermon. Reflected diffusion models. In *International Conference on Machine Learning*, pp. 22675–22701. PMLR, 2023.

Ang Lv, Xu Tan, Peiling Lu, Wei Ye, Shikun Zhang, Jiang Bian, and Rui Yan. Getmusic: Generating any music tracks with a unified representation and diffusion framework. *arXiv preprint arXiv:2305.10841*, 2023.

Lejun Min, Junyan Jiang, Gus Xia, and Jingwei Zhao. Polyffusion: A diffusion model for polyphonic score generation with internal and external controls. *arXiv preprint arXiv:2307.10304*, 2023.

Meinard Müller. *Fundamentals of music processing: Audio, analysis, algorithms, applications*, volume 5. Springer, 2015.

Alexander Quinn Nichol and Prafulla Dhariwal. Improved denoising diffusion probabilistic models. In *International conference on machine learning*, pp. 8162–8171. PMLR, 2021.

Zachary Novack, Julian McAuley, Taylor Berg-Kirkpatrick, and Nicholas J Bryan. Ditto: Diffusion inference-time t-optimization for music generation. *arXiv preprint arXiv:2401.12179*, 2024.

Yi Ren, Jinzheng He, Xu Tan, Tao Qin, Zhou Zhao, and Tie-Yan Liu. Popmag: Pop music accompaniment generation. In *Proceedings of the 28th ACM international conference on multimedia*, pp. 1198–1206, 2020.

Chitwan Saharia, William Chan, Saurabh Saxena, Lala Li, Jay Whang, Emily L Denton, Kamyar Ghasemipour, Raphael Gontijo Lopes, Burcu Karagol Ayan, Tim Salimans, et al. Photorealistic text-to-image diffusion models with deep language understanding. *Advances in neural information processing systems*, 35:36479–36494, 2022.

Jiaming Song, Chenlin Meng, and Stefano Ermon. Denoising diffusion implicit models. *arXiv preprint arXiv:2010.02502*, 2020a.

Jiaming Song, Qinsheng Zhang, Hongxu Yin, Morteza Mardani, Ming-Yu Liu, Jan Kautz, Yongxin Chen, and Arash Vahdat. Loss-guided diffusion models for plug-and-play controllable generation. In *International Conference on Machine Learning*, pp. 32483–32498. PMLR, 2023.

Yang Song and Stefano Ermon. Generative modeling by estimating gradients of the data distribution. *Advances in neural information processing systems*, 32, 2019.

Yang Song and Stefano Ermon. Improved techniques for training score-based generative models. *Advances in neural information processing systems*, 33:12438–12448, 2020.

Yang Song, Jascha Sohl-Dickstein, Diederik P Kingma, Abhishek Kumar, Stefano Ermon, and Ben Poole. Score-based generative modeling through stochastic differential equations. *arXiv preprint arXiv:2011.13456*, 2020b.

Dimitri von Rütte, Luca Biggio, Yannic Kilcher, and Thomas Hofmann. Figaro: Controllable music generation using learned and expert features. In *The Eleventh International Conference on Learning Representations*, 2023.

Ziyu Wang, Ke Chen, Junyan Jiang, Yiyi Zhang, Maoran Xu, Shuqi Dai, Xianbin Gu, and Gus Xia. Pop909: A pop-song dataset for music arrangement generation. *Proceedings of 21st International Conference on Music Information Retrieval, ISMIR*, 2020a.

Ziyu Wang, Dingsu Wang, Yixiao Zhang, and Gus Xia. Learning interpretable representation for controllable polyphonic music generation. *Proceedings of 21st International Conference on Music Information Retrieval, ISMIR*, 2020b.

Ziyu Wang, Lejun Min, and Gus Xia. Whole-song hierarchical generation of symbolic music using cascaded diffusion models. *arXiv preprint arXiv:2405.09901*, 2024.

Chen Zhang, Yi Ren, Kejun Zhang, and Shuicheng Yan. Sdmuse: Stochastic differential music editing and generation via hybrid representation. *IEEE Transactions on Multimedia*, 2023a.

Lvmin Zhang, Anyi Rao, and Maneesh Agrawala. Adding conditional control to text-to-image diffusion models. In *Proceedings of the IEEE/CVF International Conference on Computer Vision*, pp. 3836–3847, 2023b.

## A Summary of non-standard notations

Table 2: Summary of Notations

Notation	Type	Description
<b>Piano Roll-like Matrices</b>		
$M, \mathbf{M}, M^i$	discrete	Fixed/random/samples of piano roll in $\{0, 1\}^{L \times H}$ .
$\widehat{M}$	discrete	Estimated or generated piano roll
$\tilde{M}$	discrete	Generated piano roll with fine-grained sampling guidance
$M^{\text{cond}}$	discrete	The piano roll representing fine-grained conditions.
$X, \mathbf{X}, X^i$	continuous	Fixed/random/samples of continuous approximation of piano roll.
$\widehat{X}, \widehat{X}_0$	continuous	Estimated or generated value of $X$ , diffusion output.
$\tilde{X}_0, \tilde{X}_t$	continuous	Diffusion samples with fine-grained sampling guidance
<b>Textural Conditions or Guidance (abstract)</b>		
$\mathcal{K}, \mathcal{K}(l)$	condition/control	Key-signature condition or control for entire piano roll/at time $l$ .
$\mathcal{C}, \mathcal{C}(l)$	condition	Chord condition.
$\mathcal{R}, \mathcal{R}(l)$	condition	Rhythmic condition.
$\mathcal{B}, \mathcal{B}(l)$	control	Rhythmic control.
<b>Set of Indexes</b>		
$l$	$\subset [1, L]$	set of time values.
$h, \mathbf{h}(l)$	$\subset [1, H]$	set of pitch values (as function of $l$ ).
$\omega_{\mathcal{K}}(l)$	$\subset [1, H]$	pitch values that are out of key $\mathcal{K}$ at time $l$ .
$\gamma_{\mathcal{C}}(l)$	$\subset [1, H]$	pitch values corresponding to chord $\mathcal{C}(l)$ at time $l$ .
$\gamma_{\mathcal{R}}$	$\subset [1, L]$	onset time values corresponding to rhythm $\mathcal{R}$ .
<b>Set of Matrices</b>		
$\mathbb{W}_{\mathcal{K}}$	set of $M$	with out-of-key notes for key signature $\mathcal{K}$ .
$\mathbb{W}'_{\mathcal{K}}$	set of $X$	corresponding to set $\mathbb{W}_{\mathcal{K}}$ of $M$ .
$\mathbb{C}_{\mathcal{K}}$	set of $M$	with contexts accommodating out-of-key $\mathcal{K}$ notes.
<b>Probability and Events</b>		
$w, w_1$	event	$M$ has out-of-key notes.
$c, \bar{c}$	event	$M$ has or does not have “good contexts”
$P_M, \widehat{P}_M$	discrete probability	Probability/estimated probability regarding distribution of $M$
$p_X, \widehat{p}_X$	density	Density/estimated density regarding distribution of $X$
$\mathcal{P}, \mathcal{P}_{\delta}$	class	Distribution class of $p_X$

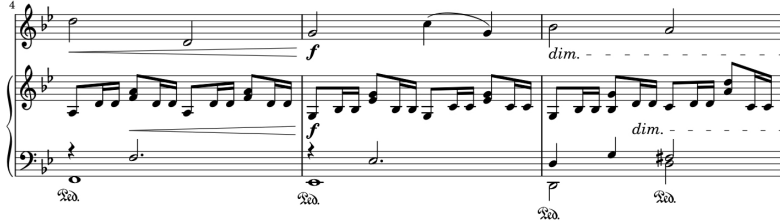
## B Examples of human-composed accompaniment



(a) Shostakovich: 5 Pieces for Two Violins and Piano: I. Prelude



(b) Beethoven: Violin Sonata No. 5 in F major, Op. 24, "Spring"



(c) Dvořák: Romance, Op. 75 No. 1 in F minor for Violin and Piano

Figure 5: Examples of piano accompaniment by human composers, sourced from IMSLP and other references, showing that the accompaniment (displayed at the bottom of each figure) can follow highly regular patterns.

## C Proof of propositions and calculation details

### C.1 Proof of Proposition 1

We first provide the detailed version of proposition 1, given as the following proposition 3. We introduce the following definitions and assumptions as foundations of the detailed proposition 3.

**Definition 1.** (*Property I*) An estimator  $\hat{p}$  constructed from  $\{\mathbf{X}_i\}_{i=1}^n$ ,  $\mathbf{X}_i \sim p(\mathbf{X})$ ,  $\mathbf{X} \in \mathbb{R}^d$  is said to satisfy property I with threshold  $q$  and constants  $A_1, A_2 \in (0, 1)$ , w.r.t. distribution  $p(\mathbf{X})$ , if  $\forall s \in \{1, 2, \dots, d\}$  and  $\forall n \in \mathbb{N}$ , we have

$$\begin{aligned} \mathbb{E} \int_{\mathbb{R}^{s-1}} d\mathbf{Y}_{s-1} \int_{(-\infty, q)} d\mathbf{X}_s \int_{\mathbb{R}^{d-s}} d\mathbf{Z}_{d-s} |\hat{p} - p|(\mathbf{Y}_{s-1}, \mathbf{X}_s, \mathbf{Z}_{d-s}) &\geq A_1 \mathbb{E}[\text{TV}(\hat{p}, p)] \\ \mathbb{E} \int_{\mathbb{R}^{s-1}} d\mathbf{Y}_{s-1} \int_{(-\infty, q)} d\mathbf{X}_s \int_{\mathbb{R}^{d-s}} d\mathbf{Z}_{d-s} |\hat{p} - p|(\mathbf{Y}_{s-1}, \mathbf{X}_s, \mathbf{Z}_{d-s}) &\leq A_2 \mathbb{E}[\text{TV}(\hat{p}, p)]. \end{aligned} \tag{14}$$

Note that

$$\text{TV}(\hat{p}, p) = \int_{\mathbb{R}^d} |\hat{p} - p|(\mathbf{X}) d\mathbf{X},$$

and property I requires that for all values of  $n$ , the estimation error is “evenly” distributed on different half-spaces separated by a given threshold  $q$ , along all dimensions  $1, 2, \dots, d$ . In other words, each half space shares a upper-and-lower-bounded proportion of estimation error, which is natural requirement for estimators, only excluding a very small proportion of extreme cases.

**Definition 2.** (Property II) Denote  $\bar{\mathcal{P}}(\hat{\mu})$  as the class of all distributions in the distribution class  $\mathcal{P}$  on which estimator  $\hat{\mu}$  satisfies property I. An estimator  $\hat{\mu}$  satisfies property II on  $\mathcal{P}$  if  $\exists$  constant  $A_3 > 0, \forall n$ ,

$$\sup_{p \in \bar{\mathcal{P}}(\hat{\mu})} \mathbb{E}_{\{x_i\}_{i=1}^n} [\text{TV}(\hat{\mu}, p)] \geq A_3 \sup_{p \in \mathcal{P}} \mathbb{E}_{\{x_i\}_{i=1}^n} [\text{TV}(\hat{\mu}, p)]. \quad (15)$$

Note that  $\bar{\mathcal{P}}(\hat{\mu})$  is a subset of  $\mathcal{P}$ , therefore, we have

$$\sup_{p \in \bar{\mathcal{P}}(\hat{\mu})} \mathbb{E}_{\{x_i\}_{i=1}^n} [\text{TV}(\hat{\mu}, p)] \leq \sup_{p \in \mathcal{P}} \mathbb{E}_{\{x_i\}_{i=1}^n} [\text{TV}(\hat{\mu}, p)].$$

Property II additionally requires that  $\sup_{p \in \bar{\mathcal{P}}(\hat{\mu})} \mathbb{E}_{\{x_i\}_{i=1}^n} [\text{TV}(\hat{\mu}, p)]$  is not too small compared with  $\sup_{p \in \mathcal{P}} \mathbb{E}_{\{x_i\}_{i=1}^n} [\text{TV}(\hat{\mu}, p)]$ . To explain, this requires the existence of a distribution  $p$  in class  $\bar{\mathcal{P}}(\hat{\mu})$  leading to a not too small distributional estimation error for  $\hat{\mu}$ , compared to the distributions in class  $\mathcal{P}$ . Since  $\bar{\mathcal{P}}(\hat{\mu})$  is constructed to satisfy property I, which is only a mild requirement for the pair  $(p, \hat{\mu})$  of distribution and estimator, property II applies to a wide range of estimators  $\hat{\mu}$ , given appropriate distribution class  $\mathcal{P}$ .

**Assumption 1.** Denote the space of density functions

$$\mathcal{P}_0 = \{p(\mathbf{X}) = f(\mathbf{X}) \exp(-C\|\mathbf{X}\|_2^2) : f \in \mathcal{L}(\mathbb{R}^{L \times H}, B), f(\mathbf{X}) \geq \alpha > 0\},$$

where  $C$  and  $\alpha$  can be any given constants, and  $\mathcal{L}(\mathbb{R}^{L \times H}, B)$  denotes the class of Lipschitz continuous functions on  $\mathbb{R}^{L \times H}$  with Lipschitz constant bounded by  $B$ .

Suppose that the density function of  $\mathbf{X}$  belongs to the following space

$$\mathcal{P}_\delta = \{p(\mathbf{X}) \in \mathcal{P}_0 \mid P_{\mathbf{M}}(\bar{\mathbf{c}}, \mathbf{w}|\mathcal{K}) = \delta\}, \quad (16)$$

where the distribution of  $\mathbf{M}$  is defined from  $\mathbf{X}$  by

$$\mathbf{M}_{lh} = \mathbf{1}\{\mathbf{X}_{lh} \geq 1/2\}.$$

The first part of assumption 1 regarding  $\mathcal{P}_0$  is adopted from Fu et al. (2024). While  $\mathcal{P}_0$  does not apply to the discrete random variable  $\mathbf{M}$ , since in practice we often approximate  $\mathbf{M}$  with continuous estimators  $\hat{\mathbf{p}}_{\mathbf{X}}$  (for their more favorable empirical properties of continuous estimators resulting from e.g., applying Gaussian noise), the underlying assumption can be given as that the discrete random variable  $\mathbf{M}$  is transformed from a continuous random variable  $\mathbf{X}$ , and distribution  $p_{\mathbf{X}}$  of  $\mathbf{X}$  is regarded as the ground truth of the continuous estimator. This justifies the use of continuous candidate distribution class  $\mathcal{P}_0$  in deriving the statistical order. Further, note that  $P_{\mathbf{M}}(\bar{\mathbf{c}}, \mathbf{w}|\mathcal{K})$  denotes the probability of containing out-of-key notes together with a “bad context” in the ground truth. We assume this probability to be low in the ground truth  $P_{\mathbf{M}}$  (otherwise there is no point analyzing how the estimated probability  $\hat{P}_{\mathbf{M}}(\bar{\mathbf{c}}, \mathbf{w}|\mathcal{K})$  can be high). Further, since our analysis focus on  $P_{\mathbf{M}}(\bar{\mathbf{c}}, \mathbf{w}|\mathcal{K})$ , we additionally enforce  $P_{\mathbf{M}}(\bar{\mathbf{c}}, \mathbf{w}|\mathcal{K})$  to restrict the class  $\mathcal{P}_0$ , forming a smaller subclass of distributions of our concern.

**Assumption 2.** Suppose that estimator  $\hat{\mathbf{p}}_{\mathbf{X}}$  satisfies property II on  $\mathcal{P}_\delta$ .

**Proposition 3.** Consider approximating  $P_{\mathbf{M}}$  with the distribution of a continuous random variable  $\mathbf{X}$ . Suppose  $n$  i.i.d. data  $\{\mathbf{X}^i\}_{i=1}^n$  come from distribution  $p_{\mathbf{X}}$ . Let  $\{\mathbf{M}^i\}_{i=1}^n$  where  $\mathbf{M}_{lh}^i = \mathbf{1}\{\mathbf{X}_{lh}^i \geq 1/2\}$  be the training data provided to the continuous estimator  $\hat{\mathbf{p}}_{\mathbf{X}}$ . Let  $\hat{P}_{\mathbf{M}}$  be derived from  $\hat{\mathbf{p}}_{\mathbf{X}}$  via the connection  $\hat{\mathbf{M}}_{lh}^i = \mathbf{1}\{\hat{\mathbf{X}}_{lh}^i \geq 1/2\}$ . With Assumptions 1 and 2 on  $\hat{\mathbf{p}}_{\mathbf{X}}$  and  $p_{\mathbf{X}}$ , we have  $\exists C > 0$ ,

$$\inf_{\hat{\mathbf{p}}_{\mathbf{X}}} \sup_{p_{\mathbf{X}} \in \mathcal{P}_\delta} \mathbb{E}_{\{\mathbf{M}^i\}_{i=1}^n} \hat{P}_{\mathbf{M}}(\bar{\mathbf{c}}, \mathbf{w}|\mathcal{K}) \geq C \cdot n^{-\frac{1}{LH+2}} - P_{\mathbf{M}}(\bar{\mathbf{c}}, \mathbf{w}|\mathcal{K}), \quad (17)$$

where  $\hat{P}_{\mathbf{M}}$  is derived from  $\hat{\mathbf{p}}_{\mathbf{X}}$  via the connection  $\hat{\mathbf{M}}_{lh}^i = \mathbf{1}\{\hat{\mathbf{X}}_{lh}^i \geq 1/2\}$ .

*Proof.* We first restate a special case of proposition 4.3 of Fu et al. (2024) as the following lemma.

**Lemma 1.** (Fu et al. (2024), proposition 4.3) Fix a constant  $C_2 > 0$ . Consider estimating a distribution  $P(\mathbf{x})$  with a density function belonging to the space

$$\mathcal{P} = \{p(\mathbf{x}) = f(\mathbf{x}) \exp(-C_2 \|\mathbf{x}\|_2^2) : f(\mathbf{x}) \in \mathcal{L}(\mathbb{R}^d, B), f(\mathbf{x}) \geq C > 0\}.$$

Given  $n$  i.i.d. data  $\{x_i\}_{i=1}^n$ , we have

$$\inf_{\hat{\mu}} \sup_{p \in \mathcal{P}} \mathbb{E}_{\{x_i\}_{i=1}^n} [\text{TV}(\hat{\mu}, P)] \gtrsim n^{-\frac{1}{d+2}},$$

where the infimum is taken over all possible estimators  $\hat{\mu}$  based on the data.

From lemma 1, since all the conditions are satisfied, we know that

$$\inf_{\hat{p}_{\mathbf{X}}} \sup_{p_{\mathbf{X}} \in \mathcal{P}_0} \mathbb{E}_{\{x_i\}_{i=1}^n} [\text{TV}(\hat{p}_{\mathbf{X}}, p_{\mathbf{X}})] \gtrsim n^{-\frac{1}{LH+2}}, \quad (18)$$

where

$$\text{TV}(\hat{p}_{\mathbf{X}}, p_{\mathbf{X}}) = \int_{\mathbb{R}^{L \times H}} |\hat{p}_{\mathbf{X}}(\mathbf{X}|\mathcal{K}) - p_{\mathbf{X}}(\mathbf{X}|\mathcal{K})| d\mathbf{X}. \quad (19)$$

From the following, all distribution and density functions are conditional distributions and densities with key signature condition  $\mathcal{K}$ , therefore, we omit the term  $\mathcal{K}$  for simplicity of notations.

Without loss of generality, suppose event  $\mathbf{w}_1$  denoting a note-out-of-key occurring at  $(l, h) = (1, 1)$  is contained in  $\mathbf{w}$ . By  $P_{\mathbf{M}}(\bar{\mathbf{c}}, \mathbf{w}) = 0$ , we have

$$\begin{aligned} \hat{P}_{\mathbf{M}}(\mathbf{w}_1) &= \int_{(\frac{1}{2}, +\infty)} dX_{11} \int_{\mathbb{R}^{L \times H-1}} d\mathbf{Y} \hat{p}_{\mathbf{X}}(X_{11}, \mathbf{Y}) \\ &\triangleq \int_{\Omega_{\mathbf{w}_1}} \hat{p}_{\mathbf{X}}(\mathbf{X}) d\mathbf{X}, \end{aligned} \quad (20)$$

where  $\mathbf{Y}$  is a  $(LH - 1)$ -dimensional variable denoting the elements in matrix  $\mathbf{X}$  excluding  $X_{11}$ . Let  $\mathbb{C}(\mathbf{w}_1)$  denotes the set of all possible realizations of piano roll  $\mathbf{M}$  with a “good context” to accommodate the out-of-key note  $\mathbf{w}_1$ , and contains the note  $\mathbf{w}_1$ . For each  $\mathbf{M} \in \mathbb{C}(\mathbf{w}_1)$ , let

$$\delta(\mathbf{M}) = \{(l, h) \in \llbracket 1, L \rrbracket \times \llbracket 1, H \rrbracket \mid M_{lh} = 1\}.$$

We have

$$\begin{aligned} \hat{P}_{\mathbf{M}}(\mathbf{c}, \mathbf{w}_1) &= \sum_{\mathbf{M} \in \mathbb{C}(\mathbf{w}_1)} \int_{(\frac{1}{2}, +\infty)^{|\delta(\mathbf{M})|}} dX_{\delta(\mathbf{M})} \int_{(-\infty, \frac{1}{2})^{L \times H - |\delta(\mathbf{M})|}} d\mathbf{Y} \hat{p}_{\mathbf{X}}(X_{\delta(\mathbf{M})}, X_{L \times H \setminus \delta(\mathbf{M})}) \\ &\triangleq \int_{\Omega_{\mathbb{C}(\mathbf{w}_1)}} \hat{p}_{\mathbf{X}}(\mathbf{X}) d\mathbf{X}, \end{aligned} \quad (21)$$

and note that  $\Omega_{\mathbb{C}(\mathbf{w}_1)} \subset \Omega_{\mathbf{w}_1}$ , we have

$$\hat{P}_{\mathbf{M}}(\bar{\mathbf{c}}, \mathbf{w}_1) = \hat{P}_{\mathbf{M}}(\mathbf{w}_1) - \hat{P}_{\mathbf{M}}(\mathbf{c}, \mathbf{w}_1) = \int_{\Omega_{\mathbf{w}_1} \setminus \Omega_{\mathbb{C}(\mathbf{w}_1)}} \hat{p}_{\mathbf{X}}(\mathbf{X}) d\mathbf{X} \quad (22)$$

To better explain and summarize equation 20, equation 21 and equation 22,  $\hat{P}_{\mathbf{M}}(\cdot)$  is always calculated by integrating  $\hat{p}_{\mathbf{X}}(\mathbf{X})$  on a corresponding domain. Similarly, for the ground truth distributions and under assumption 1 which provides  $P_{\mathbf{M}}(\bar{\mathbf{c}}, \mathbf{w}) = \delta$ , we have

$$P_{\mathbf{M}}(\bar{\mathbf{c}}, \mathbf{w}_1) = \int_{\Omega_{\mathbf{w}_1} \setminus \Omega_{\mathbb{C}(\mathbf{w}_1)}} p_{\mathbf{X}}(\mathbf{X}) d\mathbf{X} \leq \delta.$$

Therefore,

$$\begin{aligned} \hat{P}_{\mathbf{M}}(\bar{\mathbf{c}}, \mathbf{w}_1) &= \int_{\Omega_{\mathbf{w}_1} \setminus \Omega_{\mathbb{C}(\mathbf{w}_1)}} \hat{p}_{\mathbf{X}}(\mathbf{X}) d\mathbf{X} \\ &\geq \int_{\Omega_{\mathbf{w}_1} \setminus \Omega_{\mathbb{C}(\mathbf{w}_1)}} |\hat{p}_{\mathbf{X}}(\mathbf{X}) - p_{\mathbf{X}}(\mathbf{X})| - p_{\mathbf{X}}(\mathbf{X}) d\mathbf{X} \\ &\geq \int_{\Omega_{\mathbf{w}_1} \setminus \Omega_{\mathbb{C}(\mathbf{w}_1)}} |\hat{p}_{\mathbf{X}}(\mathbf{X}) - p_{\mathbf{X}}(\mathbf{X})| d\mathbf{X} - \delta \end{aligned} \quad (23)$$

By assumption 2 and definition 1 on the property of  $\hat{p}_{\mathbf{X}}$ , we have

$$\hat{P}_{\mathbf{M}}(\bar{\mathbf{c}}, \mathbf{w}_1) \geq C(A_1, A_2, LH) \cdot \text{TV}(\hat{p}_{\mathbf{X}}, p_{\mathbf{X}}) - \delta, \quad (24)$$

where  $C(A_1, A_2, LH)$  is a constant relying on  $A_1, A_2$  and  $LH$ .

By construction of packing numbers provided in the proof of proposition 4.3 of Fu et al. (2024), we note that constraint  $P_{\mathbf{M}}(\bar{\mathbf{c}}, \mathbf{w}|\mathcal{K}) = \delta$  does not change the order of the packing numbers, i.e.,  $\mathcal{P}_0$  and  $\mathcal{P}_\delta$  have the same packing numbers. Therefore, under assumptions 1 and 2, from equation 18 we have

$$\inf_{\hat{p}_{\mathbf{X}}} \sup_{p \in \mathcal{P}_\delta} \mathbb{E}_{\{\mathbf{X}_i\}_{i=1}^n} \text{TV}(\hat{p}_{\mathbf{X}}, p_{\mathbf{X}}) \gtrsim n^{-\frac{1}{LH+2}}.$$

Combining with equation 24, and noting that  $\hat{P}_{\mathbf{M}}(\bar{\mathbf{c}}, \mathbf{w}) \geq \hat{P}_{\mathbf{M}}(\bar{\mathbf{c}}, \mathbf{w}_1)$ , we have

$$\inf_{\hat{p}_{\mathbf{X}}} \sup_{p \in \mathcal{P}_\delta} \mathbb{E}_{\{\mathbf{X}_i\}_{i=1}^n} \hat{P}_{\mathbf{M}}(\bar{\mathbf{c}}, \mathbf{w}) + \delta \geq C(A_1, A_2, LH) \cdot \text{TV}(\hat{p}_{\mathbf{X}}, p_{\mathbf{X}}) \gtrsim n^{-\frac{1}{LH+2}}.$$

Therefore,  $\exists C > 0, \forall n$ ,

$$\inf_{\hat{p}_{\mathbf{X}}} \sup_{p \in \mathcal{P}_\delta} \mathbb{E}_{\{\mathbf{X}_i\}_{i=1}^n} \hat{P}_{\mathbf{M}}(\bar{\mathbf{c}}, \mathbf{w}) \geq C \cdot n^{-\frac{1}{LH+2}} - P_{\mathbf{M}}(\bar{\mathbf{c}}, \mathbf{w}).$$

which finished the proof.  $\square$

## C.2 Calculation details in 4.2

Our goal is to find the optimal solution of problem (11). Since the constraint is an element-wise constraint on a linear function of  $\varepsilon$  and the objective is separable, we can find the optimal solution by element-wise optimization. Consider the  $(l, h)$ -element of  $\varepsilon$ .

First, if  $(l, h) \notin \omega_{\mathcal{K}}(l)$ , there is no constraint on  $\varepsilon_{lh}$ . Therefore, the optimal solution of  $\varepsilon_{lh}$  is  $\hat{\varepsilon}_{\theta, lh}(\mathbf{X}_t, t|\mathcal{C}, \mathcal{R})$ .

If  $(l, h) \in \omega_{\mathcal{K}}(l)$ , the constraint on  $\varepsilon_{lh}$  is

$$X_{t, lh} - \frac{\sqrt{1 - \bar{\alpha}_t} \varepsilon_{lh}}{\sqrt{\bar{\alpha}_t}} \leq \frac{1}{2},$$

which is equivalent to

$$\varepsilon_{lh} \geq \frac{1}{\sqrt{1 - \bar{\alpha}_t}} \left( X_{t, lh} - \frac{\sqrt{\bar{\alpha}_t}}{2} \right).$$

The objective is to minimize  $\|\varepsilon_{lh} - \hat{\varepsilon}_{\theta, lh}(\mathbf{X}_t, t|\mathcal{C}, \mathcal{R})\|$ . Therefore, the optimal solution of  $\varepsilon_{lh}$  is

$$\varepsilon_{lh} = \max \left\{ \hat{\varepsilon}_{\theta, lh}(\mathbf{X}_t, t|\mathcal{C}, \mathcal{R}), \frac{1}{\sqrt{1 - \bar{\alpha}_t}} \left( X_{t, lh} - \frac{\sqrt{\bar{\alpha}_t}}{2} \right) \right\}.$$

## C.3 Proof of Proposition 2

*Proof.* Under the SDE formulation, the denoising process can take the form of a solution to stochastic differential equation (SDE):

$$d\mathbf{X}_t = - \left[ \frac{1}{2} \beta(t) \mathbf{X}_t + \beta(t) \nabla_{\mathbf{X}_t} \log p_t(\mathbf{X}_t) \right] dt + \sqrt{\beta(t)} d\bar{\mathbf{W}}_t, \quad (25)$$

where  $\beta(t/T) = T\beta_t$ ,  $\bar{\mathbf{W}}_t$  is the reverse time standard Wiener process. According to Song et al. (2020b), as  $T \rightarrow \infty$ , the solution to the SDE converges to the real data distribution  $p_0$ .

In the diffusion model,  $\nabla_{\mathbf{X}_t} \log p_t(\mathbf{X}_t)$  is approximated by  $-\varepsilon_{\theta}(\mathbf{X}_t, t) / \sqrt{1 - e^{-\int_{t_0}^t \beta(s) ds}}$ . Therefore, the approximated reverse-SDE sampling process without harmonic guidance is

$$d\hat{\mathbf{X}}_t = - \left[ \frac{1}{2} \beta(t) \hat{\mathbf{X}}_t - \beta(t) \frac{\varepsilon_{\theta}(\hat{\mathbf{X}}_t, t)}{\sqrt{1 - e^{-\int_{t_0}^t \beta(s) ds}}} \right] dt + \sqrt{\beta(t)} d\bar{\mathbf{W}}_t. \quad (26)$$

Similarly, the sampling process with fine-grained harmonic guidance is

$$d\tilde{\mathbf{X}}_t = - \left[ \frac{1}{2} \beta(t) \tilde{\mathbf{X}}_t - \beta(t) \frac{\tilde{\varepsilon}_\theta(\tilde{\mathbf{X}}_t, t)}{\sqrt{1 - e^{- \int_{t_0}^t \beta(s) ds}}} \right] dt + \sqrt{\beta(t)} d\bar{\mathbf{W}}_t, \quad (27)$$

where  $\tilde{\varepsilon}_\theta$  is defined as equation 11 and equation 12.

For simplicity, we denote the drift terms as follows:

$$\begin{aligned} f(\mathbf{X}_t, t) &= - \left[ \frac{1}{2} \beta(t) \mathbf{X}_t + \beta(t) \nabla_{\mathbf{X}_t} \log p_t(\mathbf{X}_t) \right] \\ \hat{f}(\hat{\mathbf{X}}_t, t) &= - \left[ \frac{1}{2} \beta(t) \hat{\mathbf{X}}_t - \beta(t) \frac{\varepsilon_\theta(\hat{\mathbf{X}}_t, t)}{\sqrt{1 - e^{- \int_{t_0}^t \beta(s) ds}}} \right], \\ \tilde{f}(\tilde{\mathbf{X}}_t, t) &= - \left[ \frac{1}{2} \beta(t) \tilde{\mathbf{X}}_t - \beta(t) \frac{\tilde{\varepsilon}_\theta(\tilde{\mathbf{X}}_t, t)}{\sqrt{1 - e^{- \int_{t_0}^t \beta(s) ds}}} \right]. \end{aligned}$$

Since

$$\mathbb{E}_{\mathbf{X}_t \sim p_t} [\|\varepsilon^*(\mathbf{X}_t, t) - \varepsilon_\theta(\mathbf{X}_t, t)\|^2] \leq \delta,$$

and

$$\varepsilon^*(\mathbf{X}_t, t) = -\sqrt{1 - e^{- \int_{t_0}^t \beta(s) ds}} \nabla_{\mathbf{X}_t} \log p_t(\mathbf{X}_t),$$

we have

$$\mathbb{E}_{\mathbf{X} \sim p_t} [\|f(\mathbf{X}, t) - \hat{f}(\mathbf{X}, t)\|] \leq \frac{\beta(t)}{\sqrt{1 - e^{- \int_{t_0}^t \beta(s) ds}}} \delta.$$

Now we consider  $\tilde{\varepsilon}_\theta(\tilde{\mathbf{X}}_t, t)$ , which is the solution of the optimization problem (11). In the continuous SDE case, the corresponding optimization problem becomes

$$\begin{aligned} \min_{\varepsilon} \quad & \|\varepsilon - \hat{\varepsilon}_\theta(\mathbf{X}_t, t | \mathcal{C}, \mathcal{R})\| \\ \text{s.t.} \quad & \left( \frac{\mathbf{X}_t - \sqrt{1 - e^{- \int_{t_0}^t \beta(s) ds}} \varepsilon}{e^{- \frac{1}{2} \int_{t_0}^t \beta(s) ds}} \right) \in \mathbb{R}^{L \times H} \setminus \mathbb{W}'_{\mathcal{K}}. \end{aligned} \quad (28)$$

According to Proposition 1 of Chung et al. (2022), the posterior mean of  $\mathbf{X}_0$  conditioning on  $\mathbf{X}_t$  is

$$\begin{aligned} \mathbb{E}[\mathbf{X}_0 | \mathbf{X}_t] &= \frac{1}{e^{- \frac{1}{2} \int_{t_0}^t \beta(s) ds}} \left( \mathbf{X}_t + (1 - e^{- \frac{1}{2} \int_{t_0}^t \beta(s) ds}) \nabla_{\mathbf{X}_t} \log p_t(\mathbf{X}_t) \right) \\ &= \frac{1}{e^{- \frac{1}{2} \int_{t_0}^t \beta(s) ds}} \left( \mathbf{X}_t - \sqrt{1 - e^{- \int_{t_0}^t \beta(s) ds}} \varepsilon^*(\mathbf{X}_t, t) \right). \end{aligned}$$

Since the domain of  $\mathbf{X}_0$  is  $\mathbb{R}^{L \times H} \setminus \mathbb{W}'_{\mathcal{K}}$ , which is a convex set, we know that the posterior mean  $\mathbb{E}[\mathbf{X}_0 | \mathbf{X}_t]$  naturally belongs to its domain. Therefore,  $\varepsilon^*(\mathbf{X}_t, t)$  is feasible to the problem (28). Since the optimal solution of the problem is  $\tilde{\varepsilon}_\theta(\mathbf{X}_t, t)$ , we have

$$\|\tilde{\varepsilon}_\theta(\mathbf{X}_t, t) - \varepsilon_\theta(\mathbf{X}_t, t)\| \leq \|\varepsilon^*(\mathbf{X}_t, t) - \varepsilon_\theta(\mathbf{X}_t, t)\|$$

for all  $\mathbf{X}_t$  and  $t$ . This further leads to the result that

$$\mathbb{E}_{\mathbf{X} \sim p_t} [\|\tilde{f}(\mathbf{X}, t) - \hat{f}(\mathbf{X}, t)\|] \leq \frac{\beta(t)}{\sqrt{1 - e^{- \int_{t_0}^t \beta(s) ds}}} \delta. \quad (29)$$

Moreover, since  $\tilde{\varepsilon}_\theta(\mathbf{X}_t, t)$  is essentially the projection of  $\varepsilon_\theta(\mathbf{X}_t, t)$  onto the convex set defined by the constraints in (28), and  $\varepsilon^*(\mathbf{X}_t, t)$  also belongs to the set, we know that the inner product of  $\varepsilon^*(\mathbf{X}_t, t) - \tilde{\varepsilon}_\theta(\mathbf{X}_t, t)$  and  $\varepsilon_\theta(\mathbf{X}_t, t) - \tilde{\varepsilon}_\theta(\mathbf{X}_t, t)$  is negative, which further leads to the result that

$$\|\tilde{\varepsilon}_\theta(\mathbf{X}_t, t) - \varepsilon^*(\mathbf{X}_t, t)\| \leq \|\varepsilon^*(\mathbf{X}_t, t) - \varepsilon_\theta(\mathbf{X}_t, t)\|, \quad (30)$$

which further implies

$$\mathbb{E}_{\mathbf{X} \sim p_t} [\|\tilde{f}(\mathbf{X}, t) - f(\mathbf{X}, t)\|] \leq \frac{\beta(t)}{\sqrt{1 - e^{-\int_{t_0}^t \beta(s) ds}}} \delta. \quad (31)$$

The following Girsanov's Theorem (Karatzas & Shreve (1991)) will be used (together with equation 29 and equation 31) to prove the upper bounds for the KL-divergences in our Proposition 2:

**Proposition 4.** *Let  $p_0$  be any probability distribution, and let  $Z = (Z_t)_{t \in [0, T]}$ ,  $Z' = (Z'_t)_{t \in [0, T]}$  be two different processes satisfying*

$$\begin{aligned} dZ_t &= b(Z_t, t)dt + \sigma(t)dB_t, \quad Z_0 \sim p_0, \\ dZ'_t &= b'(Z'_t, t)dt + \sigma(t)dB_t, \quad Z'_0 \sim p_0. \end{aligned}$$

We define the distributions of  $Z_t$  and  $Z'_t$  as  $p_t$  and  $p'_t$ , and the path measures of  $Z$  and  $Z'$  as  $\mathbb{P}$  and  $\mathbb{P}'$  respectively.

Suppose the following Novikov's condition:

$$\mathbb{E}_{\mathbb{P}} \left[ \exp \left( \int_0^T \frac{1}{2} \int_x \sigma^{-2}(t) \|(b - b')(x, t)\|^2 dx dt \right) \right] < \infty. \quad (32)$$

Then, the Radon-Nikodym derivative of  $\mathbb{P}$  with respect to  $\mathbb{P}'$  is

$$\frac{d\mathbb{P}}{d\mathbb{P}'}(Z) = \exp \left\{ -\frac{1}{2} \int_0^T \sigma(t)^{-2} \|(b - b')(Z_t, t)\|^2 dt - \int_0^T \sigma(t)^{-1} (b - b')(Z_t, t) dB_t \right\},$$

and therefore we have that

$$KL(p_T \| p'_T) \leq KL(\mathbb{P} \| \mathbb{P}') = \int_0^T \frac{1}{2} \int_x p_t(x) \sigma(t)^{-2} \|(b - b')(x, t)\|^2 dx dt.$$

Moreover, Chen et al. (2022) showed that if  $\int_x p_t(x) \sigma^{-2}(t) \|(b - b')(x, t)\|^2 dx \leq C$  holds for some constant  $C$  over all  $t$ , we have that

$$KL(p_T \| p'_T) \leq \int_0^T \frac{1}{2} \int_x p_t(x) \sigma(t)^{-2} \|(b - b')(x, t)\|^2 dx dt,$$

even if the Novikov's condition equation 32 is not satisfied.

According to equation 29 and equation 31, we have

$$\int_x p_t(x) \beta(t)^{-1} \|\tilde{f}(\mathbf{X}, t) - \hat{f}(\mathbf{X}, t)\| dx \leq \frac{\beta(t)}{\sqrt{1 - e^{-\int_{t_0}^t \beta(s) ds}}} \delta \leq \sup_{t \in [t_0, T]} \frac{\beta(t)}{\sqrt{1 - e^{-\int_{t_0}^t \beta(s) ds}}} \delta, \quad (33)$$

$$\int_x p_t(x) \beta(t)^{-1} \|\tilde{f}(\mathbf{X}, t) - f(\mathbf{X}, t)\| dx \leq \frac{\beta(t)}{\sqrt{1 - e^{-\int_{t_0}^t \beta(s) ds}}} \delta \leq \sup_{t \in [t_0, T]} \frac{\beta(t)}{\sqrt{1 - e^{-\int_{t_0}^t \beta(s) ds}}} \delta. \quad (34)$$

Therefore, we can apply Proposition 4 to obtain upper bounds for the KL-divergences, which leads to

$$\begin{aligned} KL(\tilde{p}_{t_0} \| \hat{p}_{t_0}) &\leq \int_{t_0}^T \frac{1}{2} \int_x p_t(x) \beta(t)^{-1} \|\tilde{f}(\mathbf{X}, t) - \hat{f}(\mathbf{X}, t)\| dx \\ &\leq \delta \int_{t_0}^T \frac{1}{2} \frac{\beta(t)}{\sqrt{1 - e^{-\int_{t_0}^t \beta(s) ds}}} dt \end{aligned} \quad (35)$$

and

$$\begin{aligned}
\text{KL}(\tilde{p}_{t_0} | p_{t_0}) &\leq \int_{t_0}^T \frac{1}{2} \int_x p_t(x) \beta(t)^{-1} \|\tilde{f}(\mathbf{X}, t) - f(\mathbf{X}, t)\| dx \\
&\leq \delta \int_{t_0}^T \frac{1}{2} \frac{\beta(t)}{\sqrt{1 - e^{-\int_{t_0}^t \beta(s) ds}}} dt.
\end{aligned} \tag{36}$$

□

## D Details of Conditioning and Algorithms

### D.1 Mathematical formulation of textural conditions in section 4.1

Denote a chord progression by  $\mathcal{C}$ , where  $\mathcal{C}(l)$  denotes the chord at time  $l \in \llbracket 1, L \rrbracket$ . Let  $\gamma_{\mathcal{C}}(l) \subset \llbracket 1, H \rrbracket$  denote the set of pitch index  $h$  that belongs to the pitch classes included in chord  $\mathcal{C}(l)$ .<sup>11</sup>, and let  $\gamma_{\mathcal{R}} \subset \llbracket 1, L \rrbracket$  denote the set of onset time indexes corresponding to rhythmic pattern  $\mathcal{R}$ . We define the following versions of representations for the condition:

- When harmonic ( $\mathcal{C}$ ) and rhythmic ( $\mathcal{R}$ ) conditions are both provided, the corresponding conditional piano roll  $\mathbf{M}^{\text{cond}}(\mathcal{C}, \mathcal{R})$  is given element-wise by  $M^{\text{cond}}_{lh}(\mathcal{C}, \mathcal{R}) = \mathbf{1}\{l \in \gamma_{\mathcal{R}}\} \mathbf{1}\{h \in \gamma_{\mathcal{C}}(l)\}$ , meaning that the  $(l, h)$ -element is 1 if pitch index  $h$  belongs to chord  $\mathcal{C}(l)$  and there is onset notes at time  $l$ , and 0 otherwise.
- When only harmonic ( $\mathcal{C}$ ) condition is provided, the corresponding piano roll  $\mathbf{M}^{\text{cond}}(\mathcal{C})$  is given element-wise by  $M^{\text{cond}}_{lh}(\mathcal{C}) = -1 - \mathbf{1}\{h \in \gamma_{\mathcal{C}}(l)\}$ , meaning that the  $(l, h)$ -element is  $-2$  if pitch index  $h$  belongs to chord  $\mathcal{C}(l)$ , and  $-1$  otherwise.

Figure 3 provides illustrative examples of  $\mathbf{M}^{\text{cond}}(\mathcal{C}, \mathcal{R})$  and  $\mathbf{M}^{\text{cond}}(\mathcal{C})$ . The use of  $-2$  and  $-1$  (rather than 1 and 0) in the latter case ensures that the model can fully capture the distinctions between the two scenarios, as a unified model will be trained on both types of conditions.

### D.2 Additional algorithms in section 4.2

In this section, we provide the following algorithm: fine-grained sampling guidance additionally with rhythmic regularization, fine-grained sampling guidance combined with DDIM sampling.

Let  $\mathcal{B}$  denote the rhythmic regularization. Specifically, we have the following types of regularization:

- $\mathcal{B}_1$ : Requiring exactly  $N$  onset of a note at time position  $l$ , i.e.,  $\sum_{h \in \llbracket 1, H \rrbracket} M_{lh} = N$
- $\mathcal{B}_2$ : Requiring at least  $N$  onsets at time position  $l$ , i.e.,  

$$\exists \mathbf{h} \subset \llbracket 1, H \rrbracket, \text{ or } \exists \mathbf{h} \subset \llbracket 1, H \rrbracket \setminus \omega_{\mathcal{C}}(l) \text{ if harmonic regularization is jointly included}$$
  
such that  $M_{lh} = 1$ , and  $|\mathbf{h}| \geq N$
- $\mathcal{B}_3$ : Requiring no onset of notes at time position  $l$ , i.e.,  $\forall h \in \llbracket 1, H \rrbracket, M_{lh} = 0$

Let the set of  $\mathbf{M}$  satisfying a specific regularization  $\mathcal{B}$  be denoted as  $\mathbb{M}_{\mathcal{B}}$ , and the corresponding set of  $\mathbf{X}$  be denoted as  $\tilde{\mathbb{M}}_{\mathcal{B}}$ , note that this includes the case where multiple requirements are satisfied, resulting in

$$\tilde{\mathbb{M}}_{\mathcal{B}} = \tilde{\mathbb{M}}_{\mathcal{B}_1, \mathcal{B}_2, \dots} = \tilde{\mathbb{M}}_{\mathcal{B}_1} \cap \tilde{\mathbb{M}}_{\mathcal{B}_2} \cap \dots$$

The correction of predicted noise score is then formulated as

$$\begin{aligned}
\tilde{\varepsilon}_{\theta}(\mathbf{X}_t, t | \mathcal{C}, \mathcal{R}) &= \arg \min_{\varepsilon} \|\varepsilon - \hat{\varepsilon}_{\theta}(\mathbf{X}_t, t | \mathcal{C}, \mathcal{R})\| \\
\text{s.t. } & \left( \frac{\mathbf{X}_t - \sqrt{1 - \bar{\alpha}_t} \varepsilon}{\sqrt{\bar{\alpha}_t}} \right) \in \tilde{\mathbb{M}}_{\mathcal{B}}.
\end{aligned} \tag{37}$$

<sup>11</sup>For example, when  $\mathcal{C}(l) = \text{C major}$  (consisting of pitch classes C, E and G),  $\gamma_{\mathcal{C}}$  includes all pitch values corresponding to the three pitch classes across all octaves.

Further, we can perform predicted noise score correction with joint regularization on rhythm and harmony, resulting in the corrected noise score

$$\begin{aligned} \tilde{\varepsilon}_\theta(\mathbf{X}_t, t | \mathcal{C}, \mathcal{R}) &= \arg \min_{\varepsilon} \|\varepsilon - \hat{\varepsilon}_\theta(\mathbf{X}_t, t | \mathcal{C}, \mathcal{R})\| \\ \text{s.t. } & \left( \frac{\mathbf{X}_t - \sqrt{1 - \bar{\alpha}_t} \varepsilon}{\sqrt{\bar{\alpha}_t}} \right) \in (\mathbb{R}^{L \times H} \setminus \mathbb{W}_\mathcal{K}) \cap \tilde{\mathbb{M}}_\mathcal{B}. \end{aligned} \quad (38)$$

We for example provide a element-wise solution of  $\tilde{\varepsilon}_\theta(\mathbf{X}_t, t | \mathcal{C}, \mathcal{R})$  defined by problem (37). For given  $l$ , suppose  $\mathcal{B}(l)$  takes the form of  $\mathcal{B}_2$ , for simplicity take  $N = 1$ . This gives  $\tilde{\varepsilon}_{\theta, lh} = \hat{\varepsilon}_{\theta, lh}$  if  $\max_h \mathbb{E}[\mathbf{X}_0 | \mathbf{X}_t]_{hl} \geq \frac{1}{2}$  and  $\mathbb{E}[\mathbf{X}_0 | \mathbf{X}_t]_{hl} = \frac{1}{2}$ ,  $h = \arg \max_h \mathbb{E}[\mathbf{X}_0 | \mathbf{X}_t]_{hl}$ , i.e.,

$$\tilde{\varepsilon}_{\theta, lh} = \frac{1}{\sqrt{1 - \bar{\alpha}_t}} \left( X_{t, lh} - \frac{\sqrt{\bar{\alpha}_t}}{2} \right),$$

if  $\max_h \mathbb{E}[\mathbf{X}_0 | \mathbf{X}_t]_{hl} < \frac{1}{2}$ . The correction applied to predicted  $\mathbf{X}_0$  ( $\mathbb{E}[\mathbf{X}_0 | \mathbf{X}_t]$ ) is illustrated in the following Figure 6.

---

**Algorithm 2:** DDPM sampling with fine-grained textural guidance

---

**Input:** Input parameters: forward process variances  $\beta_t$ ,  $\bar{\alpha}_t = \prod_{s=1}^t \beta_s$ , backward noise scale  $\sigma_t$ , chord condition  $\mathcal{C}$ , key signature  $\mathcal{K}$ , rhythmic condition  $\mathcal{R}$ , rhythmic guidance  $\mathcal{B}$   
**Output:** generated piano roll  $\tilde{\mathbf{M}} \in \{0, 1\}^{L \times H}$

```

1  $\mathbf{X}_T \sim \mathcal{N}(0, \mathbf{I})$ ;
2 for  $t = T, T-1, \dots, 1$  do
3   | Compute guided noise prediction  $\hat{\varepsilon}_\theta(\mathbf{X}_t, t | \mathcal{C}, \mathcal{R})$ ;
4   | Perform noise correction: derive  $\tilde{\varepsilon}_\theta(\mathbf{X}_t, t | \mathcal{C}, \mathcal{R})$  optimization equation 38;
5   | Compute  $\tilde{\mathbf{X}}_{t-1}$  by plugging the corrected noise  $\tilde{\varepsilon}_\theta(\mathbf{X}_t, t | \mathcal{C}, \mathcal{R})$  into equation 2
6 end
7 Convert  $\tilde{\mathbf{X}}_0$  into piano roll  $\tilde{\mathbf{M}}$ 
8 return output;
```

---

We additionally remark that the fine-grained sampling guidance is empirically effective with the DDIM sampling scheme, which drastically improves the generation speed. Specifically, select subset  $\{\tau_i\}_{i=1}^m \subset \llbracket 1, T \rrbracket$ , and denote

$$\mathbf{X}_{\tau_{i-1}} = \sqrt{\bar{\alpha}_{\tau_{i-1}}} \left( \frac{\mathbf{X}_t - \sqrt{1 - \bar{\alpha}_{\tau_i}} \hat{\varepsilon}_\theta(\mathbf{X}_{\tau_i}, \tau_i)}{\sqrt{\bar{\alpha}_{\tau_i}}} \right) + \sqrt{1 - \bar{\alpha}_{\tau_{i-1}} - \sigma_{\tau_i}^2} \hat{\varepsilon}_\theta(\mathbf{X}_{\tau_i}, \tau_i) + \sigma_{\tau_i} \varepsilon_{\tau_i},$$

we similarly perform the DDIM noise correction

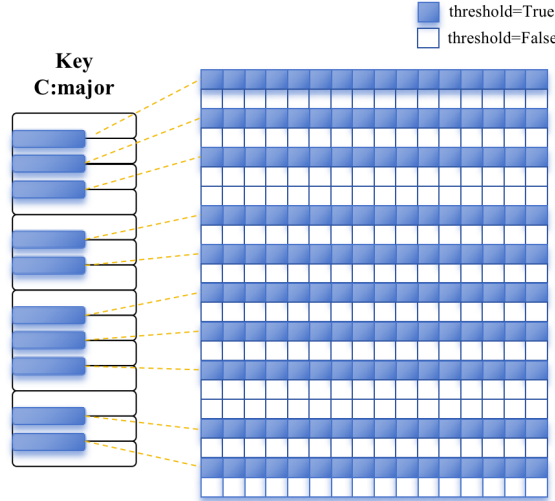
$$\begin{aligned} \tilde{\varepsilon}_\theta(\mathbf{X}_{\tau_i}, \tau_i | \mathcal{C}, \mathcal{R}) &= \arg \min_{\varepsilon} \|\varepsilon - \hat{\varepsilon}_\theta(\mathbf{X}_{\tau_i}, \tau_i | \mathcal{C}, \mathcal{R})\| \\ \text{s.t. } & \left( \frac{\mathbf{X}_t - \sqrt{1 - \bar{\alpha}_{\tau_i}} \varepsilon}{\sqrt{\bar{\alpha}_{\tau_i}}} \right) \in (\mathbb{R}^{L \times H} \setminus \mathbb{W}_\mathcal{K}) \cap \tilde{\mathbb{M}}_\mathcal{B}. \end{aligned}$$

on each step  $i$ .

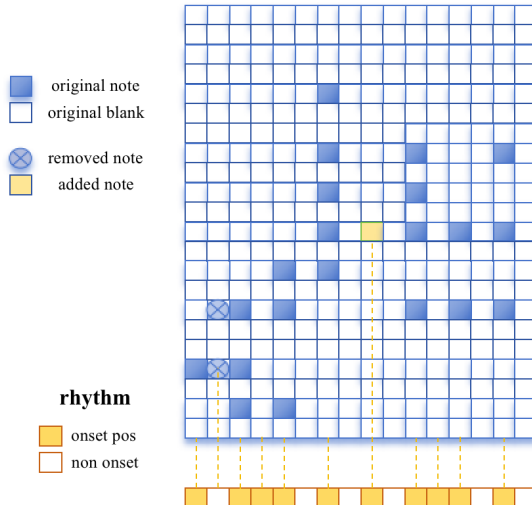
## E Comparison with Related Works

We provide a detailed comparison between our method and two related works in controlled diffusion models with constrained or guided intermediate sampling steps:

**Comparison with reflected diffusion models** In Lou & Ermon (2023), a bounded setting is used for both the forward and backward processes, ensuring that the bound applies to the training objective as well as the entire sampling process. In contrast, we do not adopt the framework of bounded Brownian motion, because we do not require the entire sampling process to be bounded within a given domain; instead, we only enforce that the final sample outcome aligns with the constraint. While Lou & Ermon (2023) enforces thresholding on  $\mathbf{X}_t$  in both forward and backward processes, our approach is to perform a thresholding-like projection method on the predicted noise  $\varepsilon_\theta(\mathbf{X}_t, t)$ , interpreted as noise correction.



(a) Fine-grained control for  $\mathbb{E}[\mathbf{X}_0 | \mathbf{X}_t] \in \mathbb{R}^{L \times H} \setminus \mathbb{W}'_{\mathcal{K}}$ . The colored spots denote places that we require  $\mathbb{E}[\mathbf{X}_0 | \mathbf{X}_t]_{lh} \leq \frac{1}{2}$



(b) Fine-grained control for  $\mathbb{E}[\mathbf{X}_0 | \mathbf{X}_t] \in \mathbb{W}'_{\mathcal{B}}$ . Original notes are removed at  $l$  if  $\mathcal{B}_3$  is applied. Otherwise if  $\mathcal{B}_1$  is applied and currently no note exists, the “most likely notes” (i.e., at  $h = \arg \max \mathbb{E}[\mathbf{X}_0 | \mathbf{X}_t]_{lh}$ ) are added.

Figure 6: Illustration of fine-grained control on predicted  $\mathbf{X}_0$ .

**Comparison with non-differentiable rule guided diffusion** Huang et al. (2024) guides the output with musical rules by sampling multiple times at intermediate steps, and continuing with the sample that best fits the musical rule, producing high-quality, rule-guided music. Our work centers on a different aspect, prioritizing precise control to tackle the challenges of accuracy and regularization in symbolic music generation. Also, we place additional emphasis on sampling speed, ensuring stable generation of samples within seconds to facilitate interactive music creation and improvisation.

## F Detailed Data Representation

The two-channel version of piano roll with both harmonic and rhythm conditions ( $\mathbf{M}^{\text{cond}}(\mathcal{C}, \mathcal{R})$ ) and with harmonic condition ( $\mathbf{M}^{\text{cond}}(\mathcal{C})$ ) with onset and sustain are represented as:

- $\mathbf{M}^{\text{cond}}(\mathcal{C}, \mathcal{R})$ : In the first channel, the  $(l, h)$ -element is 1 if there are onset notes at time  $l$  and pitch index  $h$  belongs to the chord  $\mathcal{C}(l)$ , and 0 otherwise. In the second channel, the  $(l, h)$ -element is 1 if pitch index  $h$  belongs to the chord  $\mathcal{C}(l)$  and there is no onset note at time  $l$ .
- $\mathbf{M}^{\text{cond}}(\mathcal{C})$ : In both channels, the  $(l, h)$ -element is 1 if pitch index  $h$  belongs to the chord  $\mathcal{C}(l)$ , and 0 otherwise.

In each diffusion step  $t$ , the model input is a concatenated 4-channel piano roll with shape  $4 \times L \times 128$ , where the first two channels correspond to the noisy target  $\mathbf{X}_t$  and the last two channels correspond to the condition  $\mathbf{M}^{\text{cond}}$  (either  $\mathbf{M}^{\text{cond}}(\mathcal{C}, \mathcal{R})$  or  $\mathbf{M}^{\text{cond}}(\mathcal{C})$ ). The output is the noise prediction  $\hat{\varepsilon}_\theta$ , which is a 2-channel piano roll with the same shape as  $\mathbf{X}_t$ . For the accompaniment generation experiments, we provide melody as an additional condition, which is also represented by a 2-channel piano roll with shape  $2 \times L \times 128$ , with the same resolution and length as  $\mathbf{X}$ . The melody condition is also concatenated with  $\mathbf{X}_t$  and  $\mathbf{M}^{\text{cond}}$  as model input, which results in a full 6-channel matrix with shape  $6 \times L \times 128$ .

## G Discussion

The role of generative AI in music and art remains an intriguing question. While AI has demonstrated remarkable performance in fields such as image generation and language processing, these domains possess two characteristics that symbolic music lacks: an abundance of training data and well-designed objective metrics for evaluating quality. In contrast, for music, it is even unclear whether it is necessary to set the goal as generating compositions that closely resemble<sup>12</sup> some “ground truth”.

In this work, we apply fine-grained sampling control to eliminate out-of-key notes, ensuring that generated music adheres to the most common harmonies and chromatic progressions. This approach allows the model to consistently and efficiently produce music that is (in some ways) “pleasing to the ear”. While suitable for the task of quickly creating large amounts of mediocre pieces, such models are never capable of replicating the artistry of a real composer, of creating sparkles with unexpected “wrong” keys. Nevertheless, are they supposed to?

---

<sup>12</sup>or, in what sense?